1/27

ANALYSIS OF NICHE STUDIES AND DEVELOPMENT OF BASES FOR TOTAL-SYSTEM PERFORMANCE ASSESSMENT SEEPAGE PARAMETERS

Prepared for

Nuclear Regulatory Commission
Contract NRC–02–97–009

Prepared by

Debra L. Hughson
Lauren B. Browning
Randall W. Fedors

Center for Nuclear Waste Regulatory Analyses
San Antonio, Texas

March 2000

2/27

ABSTRACT

Field studies conducted by the U.S. Department of Energy (DOE) in the niches and alcoves of the Exploratory Studies Facility at the Yucca Mountain (YM)site are briefly reviewed and models calibrated to these studies are critiqued. Comments reported here of DOE field tests and models support the criticism from the members of the DOE Drift Seepage Peer Review panel. The bulk of this report, however, describes a conceptual model of flow through unsaturated rocks of the Topopah Spring Tuff and derives estimates of parameters for seepage into emplacement drifts to be used in independent the Nuclear Regulatory Commission (NRC) performance assessments (PAs) of the potential high-level nuclear waste repository at YM, Nevada.

Results of liquid-release tests in the niches, and models calibrated using this data, support the concept of a capillary barrier formed by the underground opening. Data from secondary mineralizaton collected by the U.S. Geological Survey, however, suggests mechanisms other than a capillary barrier may control seepage into openings in YM. That is, the capillary barrier postulated from the liquid-release tests, when scaled to the size of lithophysal cavities, implies that seepage would not enter these smaller openings. Furthermore, the niche liquid-release tests were short, high flow rate tests conducted over a small length scale in the zone affected by ventilation dryout. The niche tests are therefore unlikely to be representative of closed repository conditions. The conceptual model proposed here for independent NRC PAs attempts to incorporate data of secondary mineralizaton along with radioisotope tracers and geologic features into a multi-scale bounding analysis of deep percolation and potential seepage into emplacement drifts over time-scales comparable to the period important for repository performance.

3/27

CONTENTS

4/27

FIGURES

5/27

ACKNOWLEDGMENTS

This report was prepared to document work performed by the Center for Nuclear Waste Regulatory Analyses (CNWRA) for the Nuclear Regulatory Commission (NRC) under Contract No. NRC-02-97-009. The activities reported here were performed on behalf of the NRC Office of Nuclear Material Safety and Safeguards, Division of Waste Management. The report is an independent product of the CNWRA and does not necessarily reflect the views or regulatory position of the NRC.

The authors wish to thank Walter Illman for his thorough technical reviews and useful insights, Barbara Long and Alana Woods for editorial expertise, Arturo Ramos for format review, and Budhi Sagar for programmatic review. The administrative and format support provided by Paulette Houston is also appreciated. The authors wish to acknowledge the excellent technical support given by Deborah Waiting who performed the data processing of the fracture and geological feature from the detailed line survey of the Exploratory Studies Facility (ESF).

QUALITY OF DATA AND CODE DEVELOPMENT

DATA: There are no original CNWRA-generated data contained in this report. All data used to support conclusions in this report are taken from documents published by the U.S. Department of Energy (DOE) contractors and supporting organizations who operate under the quality assurance (QA) program developed for the Yucca Mountain Project. The reader should refer to data source documents referenced throughout this report to determine data QA status. Raw data from the ESF detailed line survey were collected by the Bureau of Reclamation and U.S. Geological Survey. ESF data were transmitted from the DOE to CNWRA in August 1998. Data tracking numbers for these data are GS960708314224.008, .101, .011, .014, .003, .008, .010, .012, .020, .021, .022, .023, .024, .025, .026, and .028. Technical data information form numbers are 305556, 305554, 305624, 306645, 306017, 306284, 306298, 306299, 306509, 306510, 306511, 306512, 306513, 306514, 306515, and 306517.

CODE: Various computations in this report were performed using commercially available FORTRAN routines from Numerical Recipes (Press et al., 1992) and in the public domain from Oakridge National Laboratory available at http://www.netlib.org/. These routines are maintained in the CNWRA QA files.

1 INTRODUCTION

This report provides an independent technical review of field studies and models of water seepage into waste emplacement drifts, niches, or alcoves conducted by the U.S. Department of Energy (DOE) for assessing performance assessment (PA) of Yucca Mountain (YM), Nevada, as a potential geological repository for high-level nuclear waste. Seepage into drifts is controlled by processes with a high degree of variability and uncertainty including shallow infiltration of precipitation, deep percolation through and lateral diversion along nonwelded units of the Paintbrush Tuff, preferential flow and fast pathways through a heterogeneous network of fractures and faults, and a potential capillary barrier at the drift wall. Once inside the emplacement drift, water must enter a breach in a waste package (WP) to contact and dissolve spent nuclear fuel. This report focuses on the nature of deep percolation through fractured rock of the Topopah Spring Tuff (TSw) and the potential capillary barrier formed by the presence of the emplacement drift. Based on field tests the DOE has postulated the existence of this capillary barrier and assumed significant diversion of percolating flux away from the WP by the mechanism of lateral capillary flow in the Total System Performance Assessment for the Viability Assessment (TSPA-VA) (Civilian Radioactive Waste Management System, Management and Operating Contractor, 1998a). Tests in the niches and alcoves of the Exploratory Studies Facility (ESF) pertaining to seepage into drifts are briefly reviewed followed by comments on the DOE process model of seepage into drifts described in the Analysis/Model Report U0080 (Finsterle and Trautz, 1999). In addition, a conceptual model of deep percolation is proposed that involves statistical and geochemical analyses of potential seepage into drifts from preferential flow paths based on data of features observed in the ESF and from a distributed network of fractures inferred from secondary mineralization.

7/27

2 REVIEW OF THE U.S. DEPARTMENT OF ENERGY APPROACH

2.1 ALCOVE AND NICHE STUDIES

This section contains a brief review of tests conducted in the ESF niches relevant to seepage into drifts. This review is not comprehensive. Planned or ongoing tests in the Enhanced Characterization of Repository Block (ECRB) drift and tests conducted in the alcoves are either not covered or mentioned only briefly. Four niches and seven alcoves were constructed in the ESF at locations indicated in figure 2-1. The niches, numbered 1 through 4, will be referred to by their station locations in the ESF, consistent with DOE reports. Alcoves 1–4 are located along the North Ramp of the ESF. Alcoves 5–7 and Niches 1–4 (3566, 3650, 3107, and 4788) are located along the Main Drift of the ESF in the TSw.

Niche (1) 3566 is located at Construction Station (CS) 35 + 66 in the west wall of the ESF between the Sundance fault and a reactivated cooling joint. Elevated $^{36}Cl/Cl$ ratios, resulting from atmospheric testing of nuclear weapons, were sampled at both of these features indicating the presence of fast flow pathways. Air injection tests were conducted in three horizontal boreholes prior to excavation. Water spiked with dye was released from the middle borehole prior to excavation. Two of the three boreholes were removed during excavation, and one remains. Preexcavation water potential measurements were made in May 1997 with psychrometers.

Psychrometer 54, located 10 m from the collar of the middle borehole (M), registered a positive water potential of 0.4 m. This anomalous reading may be due at least partially to measurement error because the reported range of these instruments is from about -0.1 to -70 bars with errors ranging from a median of 5 percent up to as high as 25 percent (Klute, 1986). Some problems with psychrometer measurements are reported in Wang et al. (1999a). Even so, moisture potentials measured by psychrometers in these boreholes clearly are spatially heterogeneous, and the higher values indicate zones of increased saturation. After completion of niche excavation, a damp surface with no dye stains was observed at the far end wall, 9 m along the niche axis from its opening into the ESF. Absence of dye stains indicates this water came from a source other than the liquid released from the niche boreholes. This continuous, damp, approximately 3-m-long and 0.3-m-wide feature dried away a few hours after being exposed (Wang et al., 1997). Samples collected from this feature did not show elevated $^{36}Cl/Cl$ ratios (Hughson, 1999). After excavation, horizontal boreholes were drilled from the niche into the walls and end in a radial pattern. Humidity and water potential measuring instruments were installed by the U.S. Geological Survey (USGS), and the niche was sealed with a bulkhead for long-term monitoring.

Niche (2) 3650 is located in a relatively competent rock mass with a lower fracture density than Niche 3566. Seven horizontal boreholes were drilled prior to niche excavation for air permeability and liquid-release tests. Preexcavation liquid-release tests were conducted in the upper three and two middle boreholes by releasing typically 1 L of water with dye into 0.3-m packed-off intervals. A damp streak without dye stains, approximately 0.1-m wide, was exposed on a smooth fracture surface when a rock fell during excavation. This feature dried up within 20 min, and samples were not collected (Wang et al., 1997). Two more point damp features without dye stains were observed during the excavation of this niche. Water potentials of 0 m were measured by pyschrometers in the middle lower (ML) borehole prior to excavation, indicating saturated or nearly saturated conditions (Wang et al., 1997). Three boreholes remained after excavation. Postexcavation liquid-release tests were conducted starting mid-November 1997 and lasting for

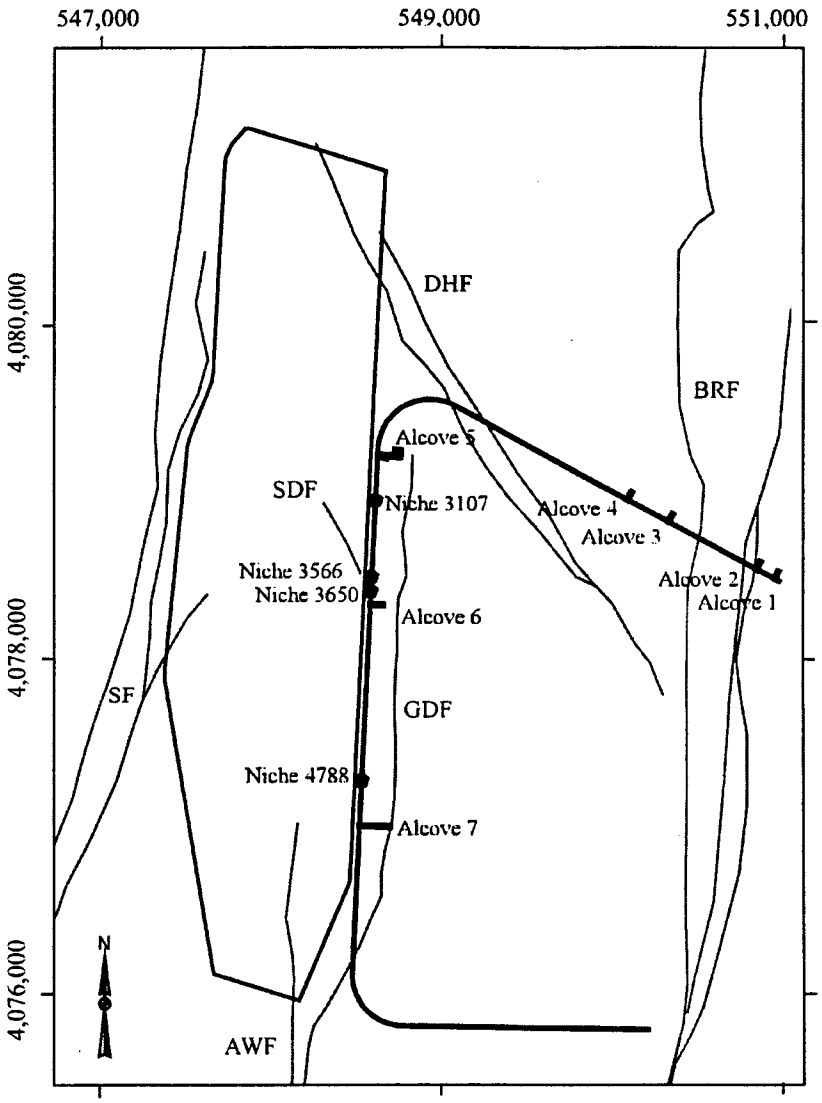

Figure 2-1. Niche and alcove locations along Exploratory Studies Facility (ESF). West of the ESF, the outline of drift area is shown. Surface traces of large faults in the vicinity of the drift area and ESF are also shown; Ghost Dance Fault (GDF), Solitario Canyon Fault (SF), Bow Ridge Fault (BRF), Drill Hole Wash Fault (DHF), Sundance Fault (SDF), and the Abandoned Wash Fault (AWF). The coordinates are in UTM NAD27 (m).

8/27

about 4 mo. Forty postexcavation, liquid-release tests were conducted at 16 different borehole intervals. Of these 16 intervals, water dripped into the capture system from 10, water appeared but did not drip in 3, and no water appeared in the remaining 3. Data from these short-duration, liquid-release tests were used as input to the seepage calibration model (section 2.2).

Niche (3) 3107 is in close proximity to the location where the ECRB crosses the ESF. Future DOE plans are to use this niche to monitor a liquid-release test between the ECRB and ESF. Seven boreholes were drilled, and air injection and liquid-release tests were conducted prior to niche excavation. Three boreholes remained after excavation, and two others, intended for monitoring moisture movement, were partially mined away. Radial boreholes were drilled after excavation in a pattern similar to niche 3566. Seven postexcavation seepage tests were conducted in this niche while the relative humidity (RH) was raised artificially to approximately 93 percent (Wang et al., 1999a).

Niche (4) 4788 is located in an exposure of the middle nonlithophysal zone of the Topopah Spring Tuff (Tptpmn). Seven boreholes were installed, and air injection and liquid-release tests were conducted prior to excavation. Four boreholes remained after excavation, and a fifth was partially mined away.

DOE also conducted fluid flow tests in five alcoves in the ESF. These tests are mentioned only briefly here as the emphasis of this report is on liquid-injection tests in the niches. Alcove 1 is the site of an ongoing, large-scale infiltration and tracer migration test conducted by the USGS in the Tiva Canyon welded tuff. Alcove 4 tests investigate flow partitioning between a fracture/fault and matrix in the Paintbrush Tuff (PTn). Alcove 5 was the site of the Single borehole Heater Test and the ongoing Drift-Scale heater Test. Alcove 6 is the site of a fracture-matrix interaction test bed in the Tptpmn. The test bed has a slot excavated below a cluster of boreholes. Wetting front detectors in monitoring boreholes and seepage collection trays in the slot were developed to evaluate partitioning of flow between matrix and fracture from injection at two borehole intervals to the slot. Passive monitoring of moisture by the USGS is ongoing in Alcove 7.

The niches were all excavated dry by an Alpine Miner in short sections to observe and photograph the distribution of dye tracer from the preexcavation liquid releases. Dye was observed along discrete fractures to depths of 2.6 m in Niches 3566 and 3650 (Wang et al., 1999a). In general, the dye was not seen to spread laterally more than about 0.5 m. Distinct, localized, high-permeability flow paths were well-defined in Niche 3650. Flow paths were predominantly downward through one or two high-angle fractures in some liquid-release tests. Other liquid-release tests showed flow through several interconnected horizontal and vertical fractures (a fracture network) with more lateral spreading. Tracer movement in clean fractures tended to have a "wiggly and fingering-like structure" (Wang et al., 1997).

Postexcavation liquid-release tests in Niche 3650 were conducted by injecting water at a constant rate into packed-off intervals of the three remaining horizontal boreholes above the niche. Water was allowed to build up to a level of 5 cm in the borehole, exiting out an overflow port if the injection rate was greater than the capacity of the formation (Wang et al., 1999a). Vertical distance between the liquid-release intervals and the niche ceiling is approximately 0.65 m. About 6 mo after these short-term liquid-release tests were completed, a 1.52 L volume of water containing tracers was released in a highly permeable zone 4.88–5.18 m from the collar of the upper middle (UM) borehole of Niche 3650 (Wang et al., 1999a). Twelve boreholes were subsequently drilled approximately 1.5 m into the ceiling of Niche 3650 to collect samples for tracer analyses. Results of these analyses showed that these sampling boreholes did not intersect the plume from this latest liquid release (Wang et al., 1999a).

Moisture potential monitoring in the ESF clearly shows a drying zone caused by ventilation extending about 1–3 m into the formation around the tunnel (Wang et al., 1999a). Visual inspection of rock samples during excavation of the niches indicated that the dye released prior to excavation appeared not to penetrate into the matrix more than a few millimeters. Subsequently, the effect of the matrix was ignored during the liquid-release tests and treated as inconsequential in calibrating the numerical models (Finsterle and Trautz, 1999). However, later analyses of samples collected from the cores concluded that "noticeable water and tracer imbibition into the surrounding matrix was observed even though the fracture flow could be fast" (Wang et al., 1999a). The conclusion from this work reported in Wang et al. (1999a) was that approximately eight percent matrix imbibition occurred during fast flow along fracture flow paths in the zone affected by ventilation dryout.

Short-term, postexcavation liquid-release tests in Niche 3566, and especially Niche 3650, form the bases for the DOE model of seepage exclusion from waste emplacement drifts and also provide the data used to calibrate a fracture continuum model of unsaturated flow around drifts. While dye tracer studies and air permeability tests are used to support the characterization of the fractured welded tuff, the field test data from liquid injections are used to make estimates of seepage threshold (Finsterle and Trautz, 1999) and flow diversion by capillarity. Estimating seepage threshold directly from liquid injections assumes the volume of injected water equals the sum of captured water and diverted water. For these niche studies, all processes that reduced the amount of captured water were lumped together and interpreted as capillary diversion.

2.2 SEEPAGE MODEL CALIBRATION

Data collected primarily from liquid-release tests in Niche 3650 have been used for model calibration (Finsterle and Trautz, 1999). Previous work on modeling of the liquid-release tests has been published (Wang et al., 1999b; Birkholzer et al., 1999) and reviewed (Chandler et al., 1999). The most recent modeling effort by Finsterle and Trautz (1999) incorporates responses to comments made by the Drift Seepage Peer Review (DSPR) panel and is the focus of commentary here.

This seepage calibration model (SCM) is 6 × 1.5 × 5 m in the x, y, and z dimensions, discretized into cubic grid blocks 0.1 m on a side. A niche 4 m wide (x dimension) and 2.5 m high (z dimension) was cut into this mesh, and a heterogeneous permeability field based on an empirical semivariogram of the postexcavation permeabilities at Niche 3650 was created by sequential indicator simulation and then mapped onto the mesh. The van Genuchten α parameter was correlated to permeability according to a scaling rule. A flux boundary condition of 3 mm/yr was applied at the top of the model; the bottom was a free-drainage boundary conditions; the sides were all no-flow boundaries; and the niche area was a prescribed pressure boundary of 1 bar. The initial condition was taken to be the equilibrium state of the model with these boundary conditions. Effective porosity and van Genuchten α parameters were then estimated by inverse model calibration to a portion of the liquid-release data using the code ITOUGH (Finsterle, 1999) with the permeability field fixed. Finsterle and Trautz (1999) acknowledge that these effective parameters are specific to this particular model but state that "[d]etermining model-related parameters from data that reveal seepage-relevant processes results in a model suitable for seepage predictions".

Despite incorporating comments from the DSPR, the proposed SCM still has significant shortcomings that render it inadequate to address or to bound the potential seepage volume and fraction of affected WPs. The SCM is based on small-scale (0.65 m), short-term (a few hours), high-volume liquid-release tests within the zone dried out by ventilation in the ESF. The SCM does not account for

moisture lost to evaporation during the field test, nor does it model matrix imbibition explicitly. Instead, the effect of matrix imbibition is reflected in an effective porosity obtained through inverse modeling. Nodal connections between the mesh elements of the SCM and the niche ceiling boundary are arbitrarily set to 0.05 m. Model calculated seepage into drifts is sensitive to the distance between the drift wall boundary and the node of the element immediately above.[1] Seepage flux will cross the drift wall boundary when saturation at a point just inside the rock formation reaches 1.0. Defining the drift crown as a reference elevation for convenience, this occurs when capillary pressure and total potential in the rock at the drift crown are zero. By connecting the mesh element node to the boundary with a nonzero vertical component, a gravity term equal to this vertical distance is added to the total potential (figure 2-2). Thus, seepage will cross the drift wall boundary when the pressure immediately inside the rock formation plus this gravitational term slightly exceeds the pressure inside the drift. This results in flux crossing the drift wall boundary at model saturation in the rock less than 1.0. Consequently, an α parameter determined by inverse modeling to match test data of seepage flux with a nonzero vertical connection distance between the drift wall boundary and the mesh element node is merely a fitting parameter that has no physical meaning or relationship to fracture characteristics such as aperture. Treating α as a fitting parameter to be adjusted through inverse modeling may still produce acceptable results but probably only if the inverse calibration is to data representing conditions expected in the repository following the thermal period. The α parameter calibrated in this manner, however, is specific to the grid used for the inverse modeling.

The SCM is based on the conceptual model of lateral flow diversion due to capillarity. The lowest seepage threshold obtained from the SCM calibrated to liquid release data was approximately 250 mm/yr. According to the theoretical model of Philip et al. (1989), seepage threshold is inversely proportional to both the α parameter and the cavity size. Using Philip's theoretical model, a cylindrical cavity of radius 2.0 m in a porous media continuum characterized by a exponential relative hydraulic conductivityα parameter of 0.015 Pa^{-1} and permeability of 2.5×10^{-13} m^2 would have a seepage threshold of 260 mm/yr. Reducing the cylindrical cavity radius to 0.25 m in the same porous media continuum increases the seepage threshold to 2,000 mm/yr. For a spherical cavity of radius 0.25 m in this porous media continuum the seepage threshold is even higher, approaching 4,000 mm/yr. These numbers are not exact nor do they necessarily apply to YM. They are intended only to illustrate that the SCM calibrated to liquid-release tests implies that water could never enter cavities the size of lithophysae. There is, however, abundant evidence that water has infiltrated into lithophysal cavities from deposits of secondary minerals. Evidence of seepage flux based secondary mineralization is discussed in chapter 4.

Not surprisingly the SCM model does a pretty good job of predicting liquid releases in Niche 3650 other than the particular tests used for inverse model calibration. This ability of the model to accurately reproduce other test results is to be expected because the model was calibrated for those conditions experienced during the liquid-release tests in Niche 3650 used for comparison (validation). Comparing the calibrated model to tests conducted in the same niche certainly does not validate the model. To be relevant to modeling seepage into drifts, the model needs to be calibrated with data collected during conditions expected in a closed repository; that is, long-term tests, at low flux rates where the air phase in fractures is near 100 percent RH, and the matrix is at its nearly saturated ambient condition. The DOE should be encouraged to conduct such tests prior to license application or as part of performance confirmation. Even in a closed repository there would be large uncertainties in seepage flux and fraction of wetted WP not

[1] Hughson, D.L., and F.T. Dodge. The effect of cavity wall irregularities on seepage exclusion from horizontal cylindrical underground openings. *Journal of Hydrology*. Accepted for publication. 2000.

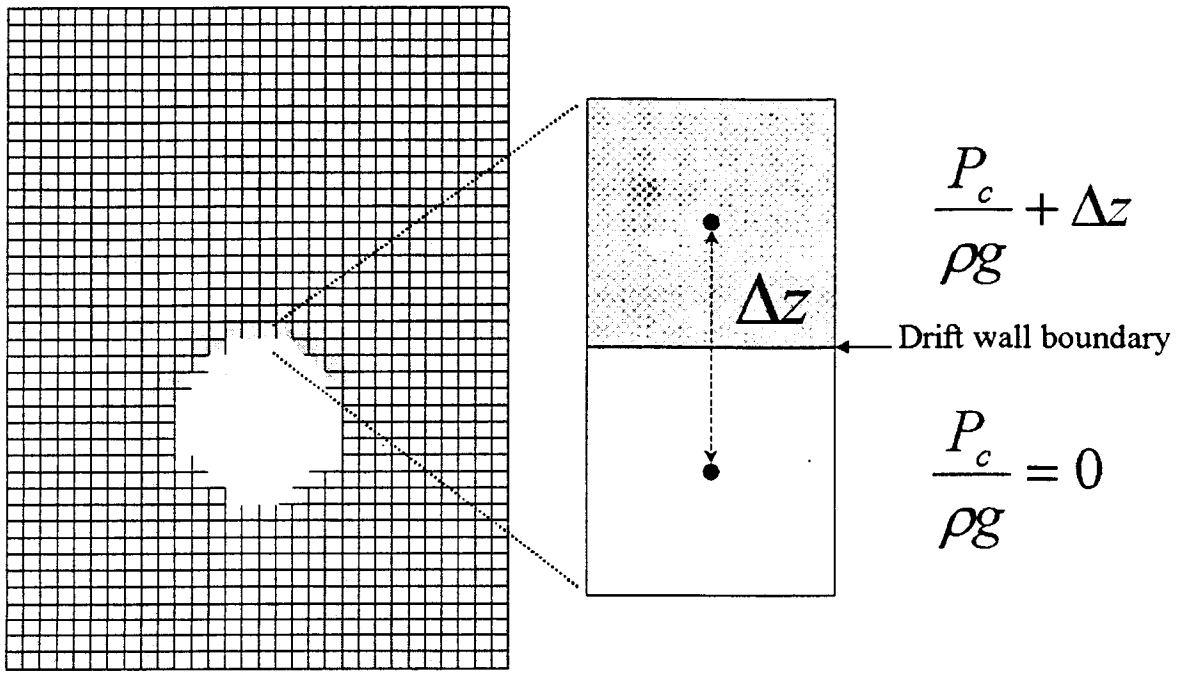

Figure 2-2. Schematic illustration showing the vertical distance, Δz, connecting the node of an element representing the drift (white box) with the node of an element representing the fractured rock continuum (gray box). Capillary pressure, P_c, at the node in the drift is fixed at zero. For a reference datum at the node in the drift element, total potential at the node in the fractured rock continuum element is $\frac{P_c}{\rho g} + \Delta z$ where ρ is density of water and g is acceleration of gravity. A nonzero Δz causes water to cross the drift wall boundary when capillary pressure at the node in the fractured rock continuum element is less than zero.

10/27

addressed by this SCM. A few of the more obvious uncertainties not addressed by the SCM are described in the following section.

2.3 UNCERTAINTIES IN U.S. DEPARTMENT OF ENERGY PREDICTIONS OF SEEPAGE INTO DRIFTS

Flow excluded from entering an open cavity by capillary forces must flow around the opening. Because relative permeability for water in an unsaturated zone (UZ) is strongly dependent on saturation, almost all this lateral flow occurs in a thin skin zone or boundary layer of higher saturation along the top boundary of the opening (Philip et al., 1989). The thickness of this boundary layer is a function of the pore size distribution parameter α characterizing the capillary strength of the porous medium. Hughson and Dodge[2] showed that a surface roughness, about the size of the boundary layer, in an otherwise smooth geometry at the crown of an underground opening in a homogeneous porous medium could decrease the seepage threshold flux by an order of magnitude. The α^{-1} parameter characterizing capillary strength of the fractures in the TSw is on the order of a few centimeters or less. Even if the emplacement drifts were to be constructed with perfectly smooth walls, Chen (1999) illustrates how an emplacement drift might look after a seismic event, and Fairhurst (1999) shows potential movement along slip planes that may affect the drift wall shape after excavation. While acknowledging their models apply only to perfectly smooth walls, the DOE currently has not addressed the potential effects of shape irregularities on seepage into emplacement drifts.

Elevated $^{36}Cl/Cl$ ratios recognized in the ESF (Fabryka-Martin et al., 1997) support the existence of localized flow pathways with travel times from the surface to the repository horizon on the order of a few decades. The number of WPs contacted by water and the flow rate onto those WPs are the important parameters for performance, not the travel times of radioisotopes from the surface. Fairly and Wu (Bodvarsson et al., 1997) used the Site-Scale Unsaturated Zone Model of Yucca Mountain to model fast transport to the repository horizon and concluded that "[b]ecause fast pathways are apparently of limited temporal and spatial extent, it seems implausible that they transmit more than a small fraction of the total flux." Fairly and Wu neglect any mention, however, of how a grid with nodes at an average spacing of 100 m is able to resolve localized preferential transport on a scale of a few centimeters to meters. Nonetheless, the present position of the Lawrence Berkeley National Laboratory and USGS researchers for the Yucca Mountain Project (YMP) appears to be that the fast pathways evident from the elevated $^{36}Cl/Cl$ ratios carry less than one percent of the flux through YM (Hughson, 1999). Members of the DSPR panel, on the other hand, point out that the presence of elevated $^{36}Cl/Cl$ ratios in the matrix pore waters of the PTn implies the existence of preferential flow pathways through the PTn, other than just along faults, and that "these fast pathways may allow significant volumes of percolating moisture to penetrate the PTn at high flux rates" (Chandler et al., 1999). The DSPR panel suggests that moisture flux through these preferential pathways could be as high as 200 mm/yr (Chandler et al., 1999). Chandler et al. (1999) do not say over what area this flux is applied or how it relates to total annual infiltration at YM. Damp features exposed during the excavation of Niches 3566 and 3650 also suggest the presence of preferential flow pathways. USGS researcher A. Flint stated that the damp feature observed in Niche 3566 must be old because elevated $^{36}Cl/Cl$ ratios were not detected (Hughson, 1999). The peer review of ^{36}Cl studies at YM, however, noted that the absence of elevated $^{36}Cl/Cl$ ratios does not imply the absence of fast flow pathways (Civilian Radioactive

[2] Hughson, D.L., and F.T. Dodge. The effect of cavity wall irregularities on seepage exclusion from horizontal cylindrical underground openings. *Journal of Hydrology*. Accepted for publication. 2000.

Waste Management System, Management and Operating Contractor, 1998b) and Murphy (1998) pointed out that the absence of elevated $^{36}Cl/Cl$ ratios may be the consequence of fast flow rather than the absence of fast paths. Clearly the presence or absence of fast flow pathways and the flux rate along these pathways is controversial and uncertain. The DSPR panel's comment that "[t]he locations at which bomb pulse ^{36}Cl have been observed in the main ESF tunnel and E-W Cross Drift ... would be the likely locations for any seeps to form" (Chandler et al., 1999) is explored in chapter 3 using a statistical approach.

Work completed for the YMP to date on seepage into drifts has ignored all coupled thermal-hydrological-mechanical-chemical (THMC) effects. Air permeability tests in Niche 3650 after excavation showed a two-order of magnitude increase compared with preexcavation air permeability tests (Wang et al., 1999a). This increase was attributed to mechanical disturbances and stress releases caused by excavation. No rock-mechanic type analyses, however, were undertaken to see how this stress release may result in widening or closing the vertical versus horizontal fractures or how this effect might translate from the scale of a niche to the scale of an emplacement drift. The thermal regime has been completely neglected in all seepage into drifts assessments to date. The TSPA-VA (Civilian Radioactive Waste Management System, Management and Operating Contractor, 1998a), for example, assumes that no water enters the drift while drift temperatures remain above boiling, and the ambient model applies once temperatures drop below boiling. To date, however, the DOE has not addressed concerns of coupled THMC processes on seepage into drifts. The DSPR report contains a list of uncertainties regarding assessment of seepage into drifts (Chandler et al., 1999). At the top of the list is uncertainty in infiltration and deep percolation. The report also states that use of uniform boundary conditions for drift-scale models smooths, and thus misrepresents, spatial variability of deep percolation flux. In addition to the uncertainties mentioned previously, the DSPR believes neglecting the matrix or assuming a small fracture-matrix interaction parameter is nonconservative, inverse models as discussed in section 2.3 are "replete with pitfalls and do not yield reliable results," neglecting vapor transport within drifts is nonconservative, representation of the multiple scales of fracture permeability heterogeneity is inadequate, and the interaction between engineered barriers and seepage into drifts has not been addressed sufficiently (Chandler et al., 1999). Most concerns about these uncertainties could be alleviated if the YMP followed the recommendations of their peer reviewers. In addition, our understanding of potential seepage into drifts would be enhanced and uncertainties reduced if the DOE should undertake long-term seepage tests for performance confirmation.

11/27

3 A PROBABILISTIC ANALYSIS OF PREFERENTIAL FLOW AND SEEPAGE INTO DRIFTS

3.1 A REVIEW OF EVIDENCE FOR PREFERENTIAL FLOW IN FRACTURED ROCK

There is substantial evidence that unsaturated flow through fractured rocks occurs in a manner not well described by the Representative Elementary Volume average of the continuum approach (Pruess et al., 1999). The stochastic continuum (SC) approach, as implemented in the SCM discussed in section 2.2, may not preserve fracture connectivity between blocks, and computation of bulk effective properties for SC blocks may produce erroneous results (Chandler et al., 1999). In addition, the SC approach used in the SCM does not account for potential localized preferential flow in high-permeability pathways. Water in high-angle fractures or fracture networks tends to flow in rivulets or fingers following localized preferential pathways. Field and laboratory evidence for preferential flow in unsaturated fractured rock is reviewed by Pruess et al. (1999), who proposed a mechanistic model of flow focusing in unsaturated fractured rock. In a review of tracer experiments in fractured rock, Tsang and Neretnieks (1998) distinguish between flow channeling caused by focusing of flow by heterogeneity along a few preferred pathways and flow fingering caused by instability of an interface between two immiscible fluids. The interface between immiscible fluids can become unstable through differences in fluid density and viscosity. In the case of water displacing air during gravity flow in a homogeneous porous medium, the interface is unstable, and fingers will develop if the flux is smaller than the saturated hydraulic conductivity (Chen et al., 1995). At YM, flow channeling and flow fingering can both focus infiltration into preferential flow paths.

Flow channeling/fingering, or rivulet flow, at YM is evidenced by the field data. An infiltration test was conducted at Fran Ridge by ponding 205 gal of blue-dyed water at the surface (Nicholl and Glass, 1995; Eaton et al., 1996). Afterward, the infiltrated rock was excavated while the fractures and blue dye stains were mapped in detail. Dye stains delineated the preferential pathways followed by the infiltrating water and showed fracture flow to the 4.5-m depth of excavation. The actual depth of infiltration was not determined. A psychrometer installed 10 m from the collar in horizontal borehole M showed readings indicating saturated or nearly saturated conditions prior to excavation of Niche 3566 (Wang et al., 1999a). Following excavation, a fracture with damp fill material was exposed at the far end of the Niche (Wang et al., 1997). Saturated water potentials of 0 m were measured in borehole ML in Niche 3650, 10 m from the collar prior to excavation (Wang et al., 1997). A few meters into the excavation, a large rock fell exposing a damp streak that apparently came from a subhorizontal fracture.

Similar observations of the effect of preferential flow have been made in other tunnels in fractured rock. Water seeps into tunnels at Rainier Mesa on the Nevada Test Site primarily from normal faults (Thordarson, 1965). A general absence of water on the Rainier Mesa tunnel walls and dry fractures interspersed among water-producing fractures was noted by Russell (1987). James Boles of the University of California gave a presentation at the Fall 1999 Meeting of the American Geophysical Union on calcite precipitates in the Mission Tunnel near Santa Barbara, California (Boles, 1999). The 6-km-long Mission Tunnel through the Santa Ynez Mountains was excavated approximately 90 yr ago to deliver water from Gibraltar Dam to Santa Barbara. The partially lined, subhorizontal tunnel cuts through steeply dipping unsaturated marine sandstone and shale at a depth of between 200 and 670 m. Flow measurements at the inlet

and outlet show approximately 1.23×10^6 m^3/yr of groundwater flow into the tunnel. Calcite precipitates indicate most of this flux is through fractures in the sandstone.

Seepage rates into a mountain tunnel in Japan were monitored continuously from May 1988 to December 1991 (Shimojima et al., 1993). The approximately 2 m × 2 m cross-section tunnel is cut into fractured sandstones and cherts near Yura, Wakayama Prefecture, Japan. Seepage was observed to appear only at specific locations on the roof of the tunnel and to drip intermittently. Lengths of the flow paths from rain infiltration to seeps at the collection locations were estimated to be approximately 10 m. By analyzing hydrographs of seepage discharge and time variations in concentration of chemical species in seepage water, Shimojima et al. (1993) were able to distinguish between rapid fissure and base flow matrix components. They defined the specific area for seepage as "[t]he rainfall catchment area contributing observed seepage per unit area."

3.2 PROPOSED CONCEPTUAL MODEL OF DEEP PERCOLATION THROUGH THE TOPOPAH SPRING TUFF

A hypothesis that flow through the UZ at YM occurs in at least three distinct modes forms the basis of the proposed conceptual model. While, in reality, a continuous spectrum of modes of flow probably exists, accounting for all scales of heterogeneity and fluxes, the separation into three modes stems from evidence of matrix flow, fracture flow, and preferential flow occurring in distinctly different scales of time and space. These three modes are hypothesized to respond to perturbations in net infiltration on distinctly different time scales. A slow flow rate through the matrix of the welded units of perhaps 1 mm/yr or less is one mode. Flow through the low permeability matrix of the welded units is postulated to respond slowly to changes in boundary conditions and can be bounded based on saturated matrix permeabilities. Another mode of flow occurs through an interconnected fracture network. Whether flow through this fracture network occurs as film flow (Tokunaga and Wan, 1997) or as more conventional flow through porous media or by a combination of mechanisms, the isotopic and textural evidence from calcite and opal deposits suggests this flux is relatively buffered from changes in net infiltration and is relatively constant through time (Paces et al., 1996, 1997, 1998a,b). Data on secondary mineralization collected from the ESF are reviewed in chapter 4. These data are used to draw inferences regarding unsaturated flow through the distributed fracture network and to estimate reasonable bounds on potential seepage into drifts from flow through the distributed fracture network. A third mode of flow occurs along connected subvertical, high-permeability zones as focused or preferential flow. This type of flow is hypothesized to be relatively independent of the matrix because of limited surface contact area and perhaps because of its transient, episodic nature (Pruess, 1999). Flow along preferential pathways is postulated to respond fairly quickly to changes in net infiltration flux. Lateral broadening of focused flow caused by dispersive mechanisms is considered negligible (Pruess, 1999). In fact, pathways for transient preferential flow are likely to become more focused with depth through a fractured rock formation because coalescence is possible, and flow path bifurcation should not occur in systems where flow is gravity dominated (Dexter, 1993). The following statistical analysis deals with this focused preferential flow as it is hypothesized to be the most likely source of water dripping onto WPs (Chandler et al., 1999).

Localized, preferential water flow by gravity drainage through heterogeneous fractured rock may show a high degree of variability through a wide range of scales making the use of volume-averaged models difficult (Pruess et al., 1999). Phenomenological models, on the other hand, abandon attempts to represent physical flow mechanisms and, instead, merely attempt to produce probabilities of possible events given

12/27

some input. The following proposed model of potential seepage into waste emplacement drifts and dripping onto WPs is such a phenomenological approach. Input from the surface infiltration models and assumptions about deep percolation through the PTn are translated into probability distributions for the number of WPs impacted by seeps and and also to form an estimate of the volumetric flow rate from those seeps. Implicit in this conceptual model are the assumptions that (i) water with the potential to drip on WPs at YM flows primarily through vertically connected, high-permeability zones as narrow rivulets, and (ii) water flowing through the matrix will not drip. The first of these assumptions is analogous to the weeps model used in earlier PAs of YM (Gauthier, 1994). The second assumption is reasonable because minimal water flows through the matrix of the welded units and the capillary strength of the matrix is high. Flux through the fracture network is considered in chapter 4 based on inferences from secondary minerals.

This probabilistic model of seepage into emplacement drifts is built on the following two key premises.

- Flow in a given seep is derived from a unique seepage catchment area.
- The probability that a given seep will drip onto a WP is statistically independent of all other seeps.

Suppose that every particle of water entering the subsurface flow system at YM were tagged. The first premise presumes that these tags would allow delineation of a distinct seepage catchment area for each discrete seep. Let

$$A_i \equiv \text{Seepage catchment area of seep } i \tag{3-1}$$

and

$$\sum_{i=1}^{N} A_i = \phi A_{\text{rep}} \tag{3-2}$$

where N is the number of discrete seeps within the area of the repository, A_{rep}, and ϕ is a factor between 0 and 1, assumed here to be 1, accounting for that portion of A_{rep} which does not contribute infiltration flux to preferential flow. While continuity of flow through the mountain must be preserved, it is not necessarily true that seepage catchment areas must sum to the total repository area. In fact, the sum of seepage catchment areas is probably less than the total repository area because some fraction of the repository area probably does not contribute infiltration to preferential flow. However, the error in this assumption is on the side of conservatism as this model will predict a few more seeps than actually may exist. Determination of the value of ϕ from topography, soil cover, and other information is left for future analyses. Physical determination of seepage catchment areas is not intended. Rather, A_i is treated as a random variable, and only the first two moments of its distribution are used.

In the absence of any knowledge other than that a seep exists somewhere with the repository block, it seems reasonable to assume that the probability this seep is located where it has the potential to drip onto a WP is

$$p = \frac{A_{t\mathrm{WP}}}{A_{\mathrm{rep}}} \tag{3-3}$$

where $A_{t\mathrm{WP}}$ is the total footprint area of all the WPs within the repository block. Assuming this probability, p, is the same for all seeps, combined with the second premise that seeps are independent, implies that the number of seeps with potential to drip onto WPs has a binomial distribution of mean Np and variance $Np(1-p)$.

Assuming that the system can be treated as quasi-steady, or with negligible storage, for deep percolation flux, q, the volumetric flux from seep, i, is estimated as

$$Q_i = qA_i - q_{\mathrm{matrix}}A_i - q_{\mathrm{net}}A_i - Q_c \tag{3-4}$$

where q_{matrix} is the flux through the matrix (assumed to be the saturated hydraulic conductivity of the matrix), q_{net} is flux through the fracture network (estimated from assumptions about secondary minerals in chapter 4), and Q_c is the volumetric flow diverted away from the WP by fracture capillarity. Analyses of data from the ESF are presented in the following section suggesting that the seepage catchment areas, A_i, can be approximately characterized as lognormally distributed with mean, $\mu_{\ln A}$, and standard deviation, $\sigma_{\ln A}$. If q is lognormally distributed, or is taken as a spatially uniform constant in a repository subarea for a particular realization, then volumetric flow rates from discrete seeps also would be lognormally distributed. Characterizing spatially variable water flux in heterogeneous porous media using a lognormal probability distribution was suggested by Chesnut (1992). Jury (1982) and Jury and Roth (1990) also found that solute transport in a number of field studies was fairly well described by a lognormal distribution. For a particular realization of a Monte Carlo type simulation, this seepage into drifts model is applied as follows. Random variables are drawn from a lognormal distribution of mean, $\mu_{\ln A}$, and standard deviation, $\sigma_{\ln A}$, until they fill the repository area. The number of seeps potentially flowing onto WPs is then drawn from a binomial distribution of mean, Np, and variance, $Np(1-p)$, and their flow rates are drawn from a lognormal distribution determined by the parameters $\mu_{\ln A}$ and $\sigma_{\ln A}$. The values of q are assumed to be given. As mentioned previously, q_{matrix} is taken to be the saturated hydraulic conductivity of the matrix, which may also be drawn from a distribution. Assumptions about the distribution of q_{net} are probably more important, are certainly problematic, and are addressed in chapter 4. Capillary diversion in high-angle fractures may or may not be significant. If the capillary strength parameter for high-angle fractures is taken as α = 1,000 m^{-1} from Wang et al. (1999a), then Q_c is likely to be small. This seepage model is presented for the entire repository area but is equally applicable on the basis of repository subareas.

3.3 SEEPAGE MODEL PARAMETER ESTIMATION

The phenomenological model for seepage into drifts presented in section 3.1 requires parameters $\mu_{\ln A}$ and $\sigma_{\ln A}$, the mean and standard deviation of the log-transformed seepage catchment areas. Estimates

of the ranges of these parameters are presented in this section based on data collected from the ESF. A plot of $^{36}Cl/Cl$ ratio for 189 samples, collected both at 200-m intervals and at specific features, versus ESF station is shown in figure 3-1. Ratios higher than $^{36}Cl/Cl = 900 \times 10^{-15}$ (+ symbols in figure 3-1) are taken as evidence of bomb pulse contamination (Murphy, 1998) indicating the presence of preferential flow paths. An empirical cumulative distribution function (CDF) of the natural log-transformed interval length, $\ln(L)$, between bomb pulse $^{36}Cl/Cl$ samples, neglecting intervals of zero length, is shown in figure 3-2 compared to a normal CDF with mean 4.0 and standard deviation 1.55. The Kolmogorov-Smirnov statistic, the largest difference between the sample CDF and the cumulative normal distribution, for these 38 data is 0.087, which has a significance of 0.92. This significance implies that the log-transformed intervals between bomb pulse $^{36}Cl/Cl$ ratios are normally distributed with at least 90 percent confidence.

Samples for ^{36}Cl analyses were collected at 200-m intervals and at locations likely to be potential preferential flow pathways such as faults and fractures. Thus the intervals between detection of bomb pulse ^{36}Cl in the ESF are probably maximum intervals between preferential flow paths because more sampling likely would detect more bomb pulse signals and reduce their spacing. Low infiltration rates probably result in widely spaced preferential flow paths. As infiltration increases, the spacings between seeps likely decreases. Minimum spacings between potential seeps may be estimated from the ESF detailed line survey data. A database of geologic features in the ESF classified as faults, shears, and fracture zones was assembled by the Center for Nuclear Waste Regulatory Analyses staff from data collected in the detailed line survey. An empirical CDF of 1,216 log-transformed intervals between these geologic features in the ESF, from CS 00 + 65 to 78 + 55, is shown in figure 3-3 compared with the cumulative normal of mean 0.87 and standard deviation 1.56. Intervals between prominent structural features in the ESF appear to be reasonably closely approximated by a lognormal distribution even though the Kolmogorov-Smirnov statistic of 0.048 has a low significance of 0.006. This low significance indicates that the lognormal distribution is only an approximation.

Lengths of the intervals between faults, shears, and fracture zone features in the ESF appear to have poor spatial correlation as indicated by the semivariogram in figure 3-4. The semivariogram was constructed by assigning the interval between two features to the ESF coordinate at the end of the interval (up triangles) and beginning of the interval (down triangles) then treating this number as a spatially distributed random variable. The sample semivariogram was calculated from the formula (Deutsch and Journel, 1992)

$$\gamma(h) = \frac{1}{2M(h)} \sum_{i=1}^{M(h)} \left(x_i - y_i\right)^2 \qquad (3\text{-}5)$$

where $M(h)$ is the number of pairs of data, x_i and y_i, in lag h. The lag interval used for calculating the semivariogram was 1.0 ± 0.5 m. The sample semivariogram in figure 3-4 indicates poor spatial correlation of intervals between prominent structural features in the ESF. Thus, intervals between features with the potential to be fast pathways for unsaturated flow will be treated here as independent, lognormally distributed, random variables.

Structural features and radioisotope data provide some information about the spacing between potential fast flow paths in the ESF, but what is needed for the proposed seepage model are the first and second moments of the distribution of seepage catchment areas. The need to relate mapped point data to areas is commonly encountered in spatial statistics, and several methods have been developed to approach this problem. A technique possibly appropriate to relating seeps (conceptualized as a point process on a map) to seepage catchment areas is known as Voronoï tesselation. The Voronoï tesselation area, or Dirchlet cell,

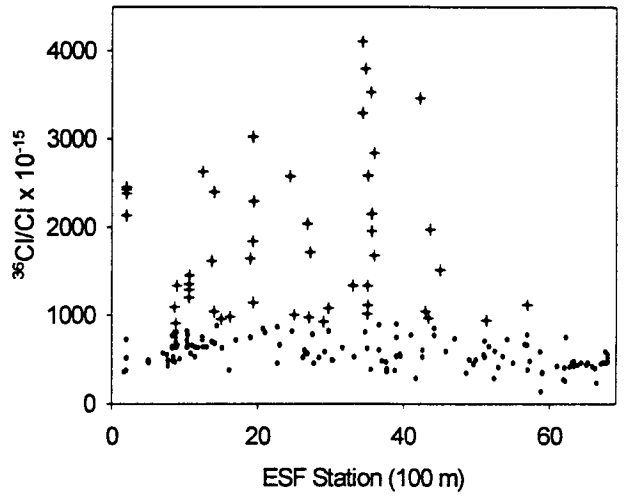

Figure 3-1. ^{36}Cl/Cl ratios from samples collected at 200-m intervals and selected geologic features in the Exploratory Studies Facility (ESF) from the North Portal to CS 67 + 60 (Fabryka-Martin et al., 1997)

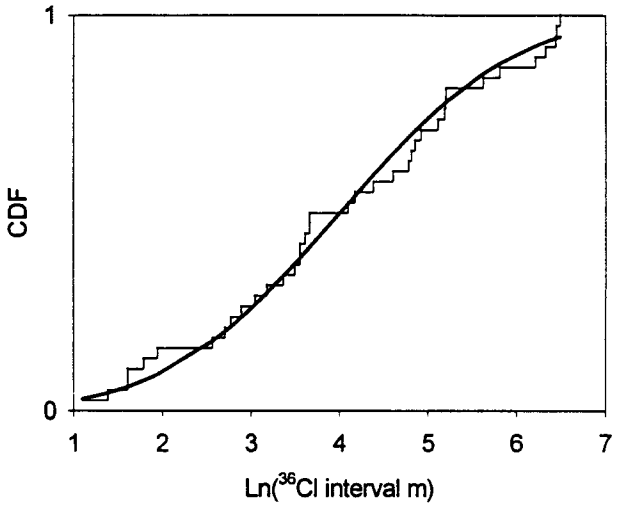

Figure 3-2. Sample cumulative distribution function (CDF) of log-transformed intervals between bomb pulse ^{36}Cl in the Exploratory Studies Facility and the cumulative normal distribution of mean 4.0 and standard deviation 1.55

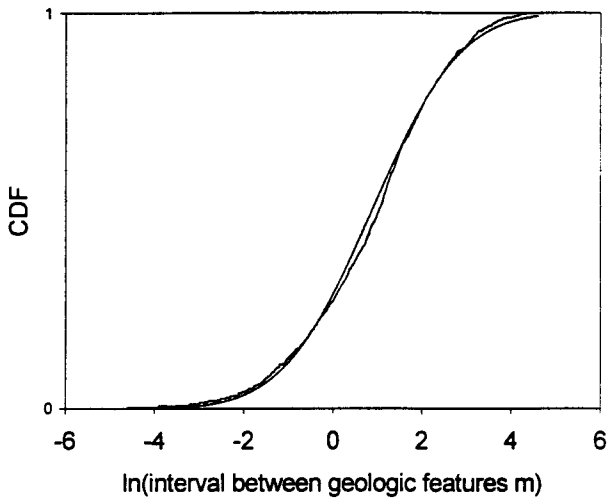

Figure 3-3. Sample cumulative distribution function of log-transformed intervals between geologic structures in the Exploratory Studies Facility identified as fault, shear, or fracture zones and the cumulative normal distribution of mean 0.87 and standard deviation 1.56

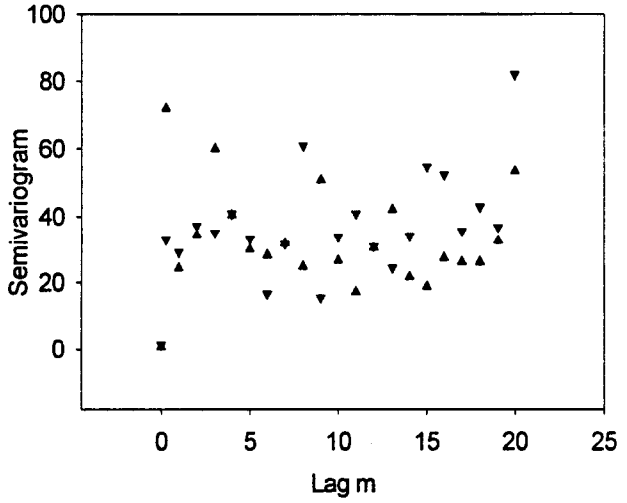

Figure 3-4. Sample semivariogram of intervals between geologic features in the Exploratory Studies Facility. See text for explanation of symbols.

surrounding a given point is defined as that part of the domain nearer to that point than to any other (Ripley, 1981). Seepage catchment areas are conceptualized as the Dirchlet cells obtained from tesselation and the points as locations of seeps. Constraining the mean and variance of seepage catchment areas by physical information, such as topography or soil cover, may substantially improve this model. Figure 3-5 shows 100 points randomly distributed in an area of x = 2,000 m and y = 1,000 m and the Dirchlet cells associated with each point generated using the code AMESH (Haukwa, 1998). Figure 3-6 shows the same area with 10,000 randomly distributed points. The relationship between the moments of point spacings, such as along the ESF, to moments of areas of the Dirchlet cells was simulated as follows. N points were randomly distributed throughout the area shown in figure 3-6 by generating the x and y coordinates uniformly on the intervals of 2,000 and 1,000 m. Areas of the Dirchlet cells were computed with AMESH, and spacings between points were taken from the x coordinates of all points falling in the region $500 \le y \le 507$ m. Figure 3-7 shows the sample CDF of log-transformed spacings (x coordinate) between points in the 7-m-wide region, ln(L), compared to a normal CDF of mean 2.93 and standard deviation 1.29. The Kolmogorov-Smirnov statistic in this case is 0.066 with a significance of 0.96. The sample CDF for log-transformed areas of the 10,000 Dirchlet cells, ln(A), in figure 3-6 is shown in figure 3-8 compared to a normal CDF of mean 5.15 and standard deviation 0.585. While the Kolmogorov-Smirnov statistic is smaller, 0.048, its significance is zero due to the large sample size of 10,000, again indicating that the lognormal assumption is only an approximation.

While the means of ln(L) between features in the ESF, (faults, shear zones, or bomb pulse ^{36}Cl) vary, their standard deviations are fairly constant. Standard deviation of ln(L) between bomb pulse ^{36}Cl signals is 1.55 and the standard deviation of ln(L) between prominent features is 1.56. The smallest standard deviation obtained in this study from the ESF line survey data was 1.22 from ln(L) between 9,513 fractures in the main (horizontal) portion of the ESF. Similar behavior was seen in simulations of the relationship between distributions of ln(A) of Dirchlet cells and ln(L) between points lying in the 7-m-wide strip. A linear relationship between the mean of ln(L) and ln(A) and the log of the number of points (or areas) generated on the plane for a simulation is seen in figure 3-9 whereas standard deviations of both ln(L) and ln(A) remain nearly constant, independent of N (figure 3-10). Fluctuations in the mean and standard deviation of ln(L) at smaller N are due to the small sample sizes of intervals falling within the 7-m-wide strip. Likewise, small variability in the mean and standard deviation of ln(A) are due to the larger sample sizes equal to N. Standard deviation of ln(L) appears to be converging to a value of around 1.25 at the largest N simulations of 60,000 while the standard deviation of ln(A) appears to be stable at about 0.59.

The simulated relationship between ln(L) and ln(A) provides some guidance for extrapolating ESF data on structural features and radioisotope evidence of fast flow paths to the parameters $\mu_{\ln A}$ and $\sigma_{\ln A}$ required by the model of section 3.2. The standard deviations of the ESF data fall within the range simulated for the means of ln(L) for smaller N and appear to converge to similar values for larger N (1.25) and larger ESF data sets (1.22 for 9,513 mapped fractures). Thus a constant parameter of about $\sigma_{\ln A} \approx 0.6$ seems reasonable. A log-linear relationship of

$$\mu_{\ln A} = (0.995)\mu_{\ln L} + 2.39 \qquad (3\text{-}6)$$

is shown in figure 3-11 where the mean of ln(L), $\mu_{\ln L}$, covers the range observed from bomb pulse ^{36}Cl intervals to prominent geologic feature intervals in data from the ESF. Realistically, the parameter $\mu_{\ln A}$ should be related to infiltration flux. During dry climate conditions, the flowing seeps would be widely spaced, and under wetter climate conditions, more of the potential conduits would be flowing and thus more closely

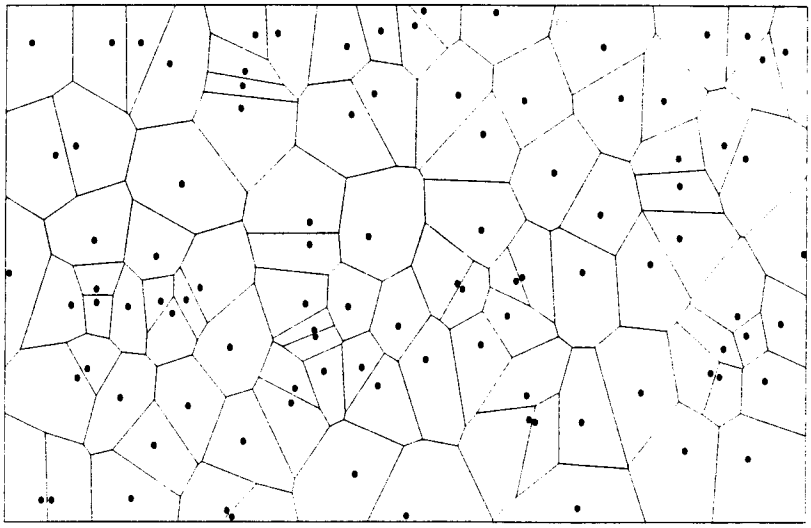

Figure 3-5. Domain used for simulating interval and area statistics illustrating 100 randomly distributed points and their associated Dirchlet cells

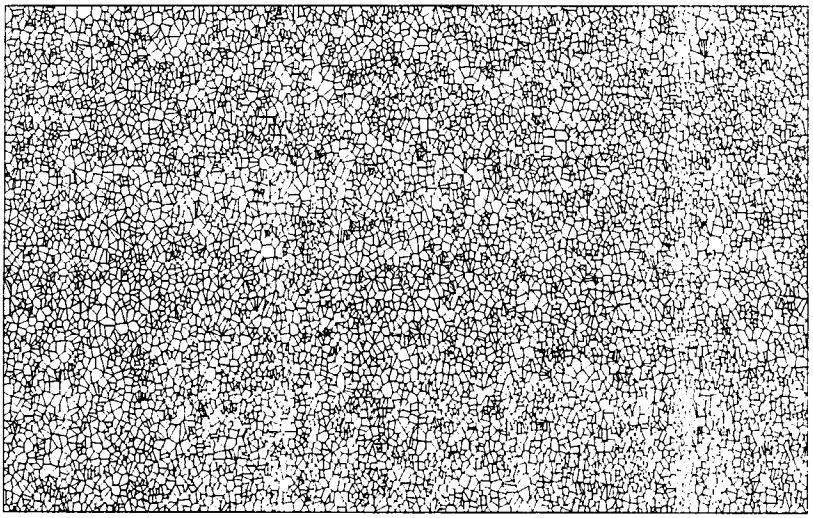

Figure 3-6. Same area as figure 3-5, but with 10,000 points and Dirchlet cells

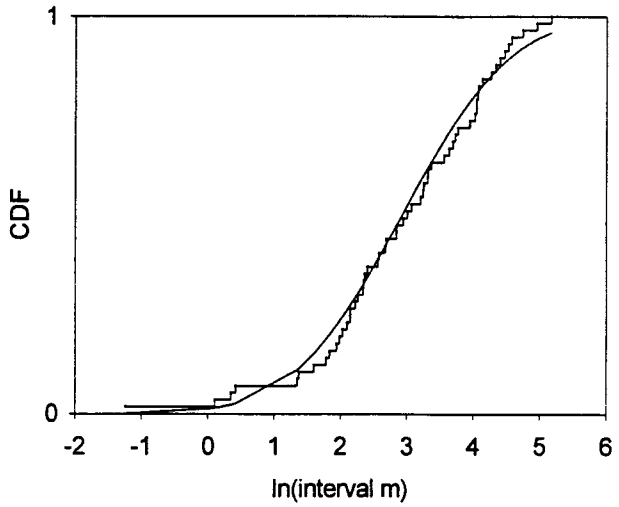

Figure 3-7. Sample cumulative distribution function (CDF) of log-transformed intervals (x coordinate) of simulated points falling within a 7-m-wide band. The cumulative normal CDF shown has mean 2.93 and standard deviation 1.29.

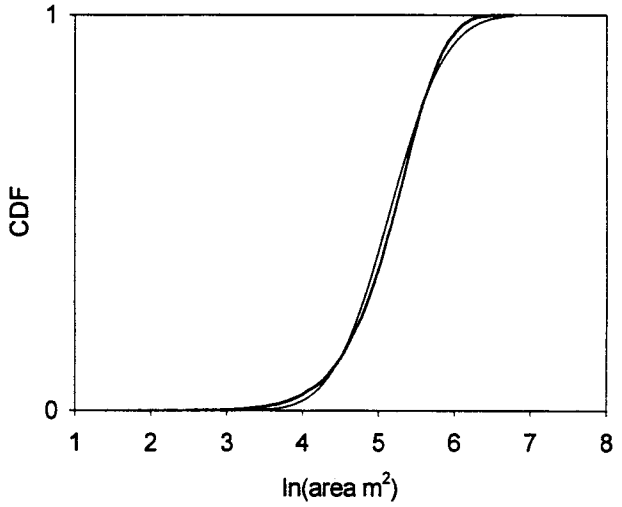

Figure 3-8. Sample cumulative distribution function of the 10,000 areas shown in figure 3-6. The cumulative normal distribution has a mean of 5.15 and standard deviation of 0.585.

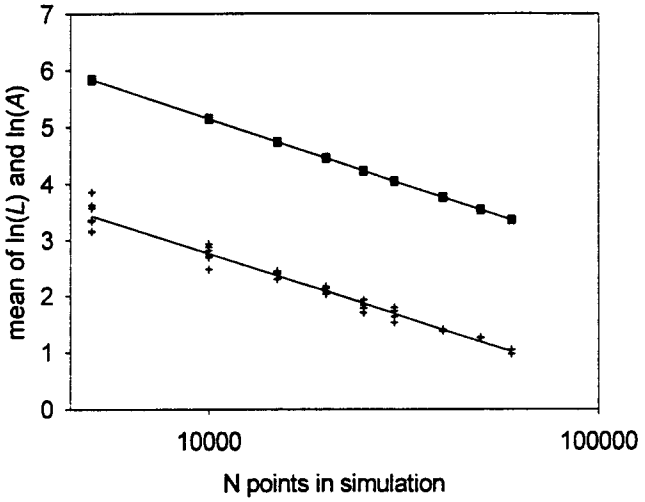

Figure 3-9. Means of simulated ln(L) (+ symbols) and simulated ln(A) (solid square symbols) showing a linear relationship with log(N)

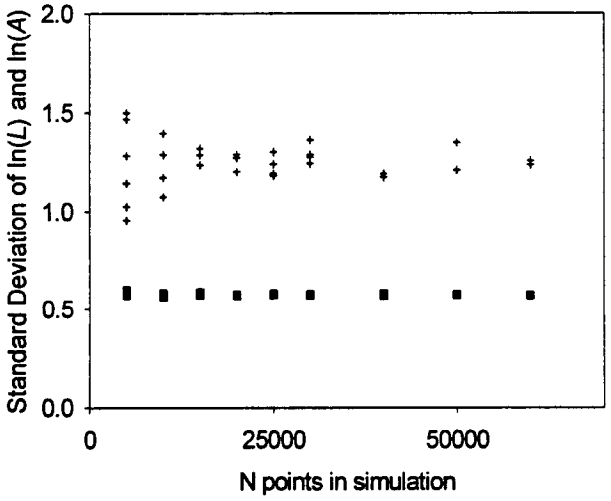

Figure 3-10. Standard deviations of simulated ln(L) (+ symbols) and ln(A) (solid square symbols) appear to be relatively constant at about 1.25 and 0.58, respectively, independent of N

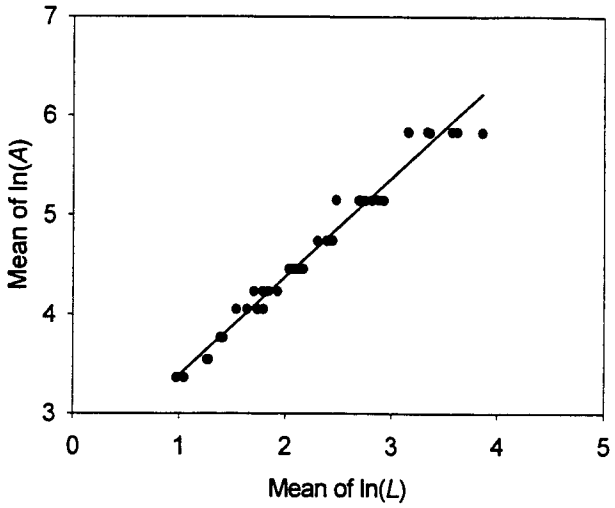

Figure 3-11. Linear relationship between simulated means of ln(L) and ln(A)

spaced. During present day climate conditions, a larger $\mu_{\ln L}$, such as obtained from intervals between bomb pulse ^{36}Cl, would be appropriate. For wetter climate conditions, more, perhaps all, of the potential fast flow paths would be carrying water, and a smaller $\mu_{\ln L}$, such as observed from the prominent structural features in the ESF, may be more appropriate.

3.4 SOME RESULTS OF THE PROBABILISTIC SEEPAGE MODEL

Repository design parameters for the Enhanced Design Alternatives II are for 10,039 WPs to be placed in 54 km of drift in an area of about 4.3×10^6 m^2. Assuming a WP width of 1.6 m gives $p \approx 0.02$. To assess the effect of preferential flow on the fraction of WPs contacted by dripping water, Monte Carlo simulations were performed by drawing ln(A_i) from a normal distribution with parameters $\mu_{\ln A}$ and $\sigma_{\ln A}$ until the repository area was filled. The number of preferential flow paths having potential to drip was then drawn from a binomial distribution with parameters of mean, Np, and variance, $Np(1-p)$. Flow rates, Q_i, from these seeps have a lognormal distribution with flux magnitudes based on assumptions about infiltration and partitioning between matrix, fracture network, and preferential flow components. Results of 1,000 Monte Carlo simulations, using $\mu_{\ln L} = 4.0$ from ^{36}Cl data, $\mu_{\ln A} = 6.37$ from Eq. (3-6), and $\sigma_{\ln A} \approx 0.6$ are shown in figure 3-12. These results suggest that, if preferential flow occurs at the frequency of bomb pulse ^{36}Cl samples in the ESF, somewhere between 80 and 160 seeps may have the potential to drip onto WPs. The corresponding F_{wet} parameter, that is, the fraction of WPs contacted by dripping water, ranges from about 0.008 to 0.016 based on the assumption that each WP is contacted by only one seep. Most of the variability in figure 3-12 results from the binomial deviate because the parameter Np only varied between about 119 and 125. An assessment of the potential flow rates from these seeps was made by assuming a total infiltration flux of 5.5 mm/yr, partitioned as 1.0 mm/yr through the welded tuff matrix, 4.0 mm/yr through the fracture network, and

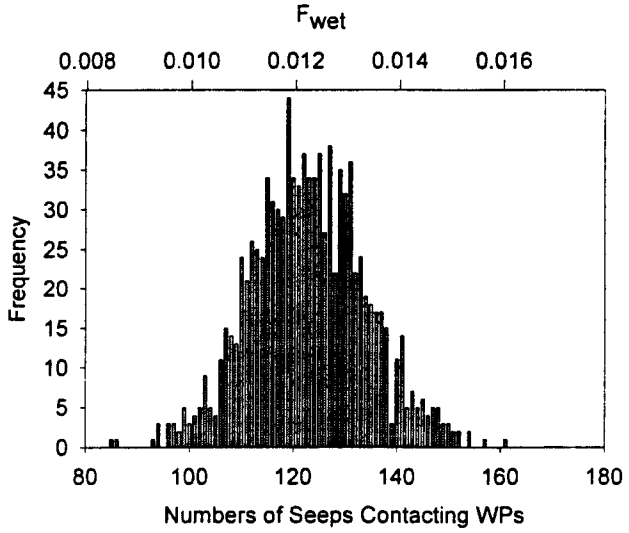

Figure 3-12. Monte Carlo simulations of numbers of seeps contacting waste packages (WPs) and fraction of wetted WPs, F_{wet}, based on intervals between bomb pulse ^{36}Cl samples in the Exploratory Studies Facility

0.5 mm/yr via preferential flow. While these fluxes are primarily illustrative, they are consistent with estimates made using a chloride mass balance approach based on precipitation and waters from the PTn and ESF, which suggest 10 percent of net infiltration flows along preferential pathways (Nuclear Regulatory Commission, 1998). A histogram of seepage flow rates from a single Monte Carlo realization is shown in figure 3-13. The geometric mean of this realization is 0.8 L/d with a minimum of about 0.12 L/d and a maximum of about 6.9 L/d.

Numbers of seeps potentially contacting WPs for wetter climate conditions were obtained from 1,000 Monte Carlo realizations based on geologic features in the ESF recognized as faults, fracture zones, or shear zones. The results using $\mu_{\ln A} = 3.26$ and $\sigma_{\ln A} \approx 0.6$ are shown in figure 3-14. In this case, the number of seeps potentially contacting WPs ranges from about 2,600 to 2,900 and the corresponding F_{wet} from about 0.26 to 0.29. A histogram of seepage flow rates from a single Monte Carlo realization assuming 26 mm/yr total infiltration, partitioned as 1 mm/yr in the matrix, 5 mm/yr in the fracture network, and 20 mm/yr in preferential flow, is shown in figure 3-15. With these assumptions, the geometric mean seepage flow rate has increased to about 1.4 L/d with a minimum of 0.15 L/d and a maximum of 17 L/d. Flow rates in figures 3-13 and 3-15 are largely illustrative. A more rigorous analysis incorporating all terms of Eq. (3-4) will be undertaken should the NRC decide to adopt this model for its TPA code. The first term in Eq. (3-4) can be based on the surface infiltration map. The second and third terms of Eq. (3-4) can be derived from the distribution of saturated matrix permeability in the welded tuff units and distribution of flux through the fracture network inferred from secondary mineralization. The last term in Eq. (3-4) can either be conservatively assumed negligible or estimated from fracture aperture and capillary rise (Hughson et al., 1999). Furthermore, constraints may be placed on the range of preferential flow rates and corresponding seepage catchment areas using recently developed constitutive mechanistic models of unsaturated fracture flow (Yang et al., 1999).

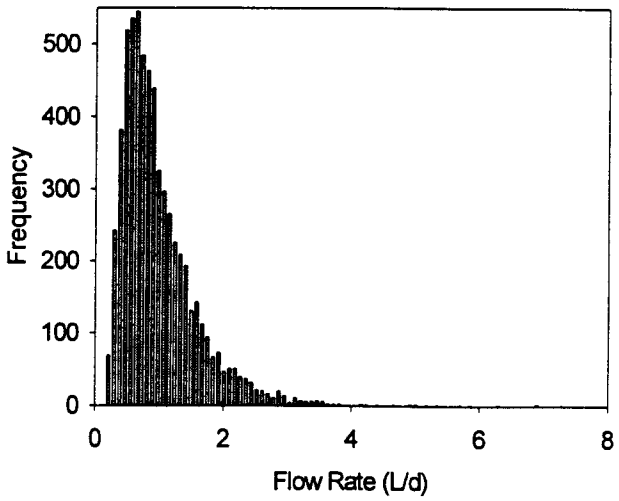

Figure 3-13. Histogram of flow rates from a single Monte Carlo realization using frequency of preferential flow based on ^{36}Cl intervals

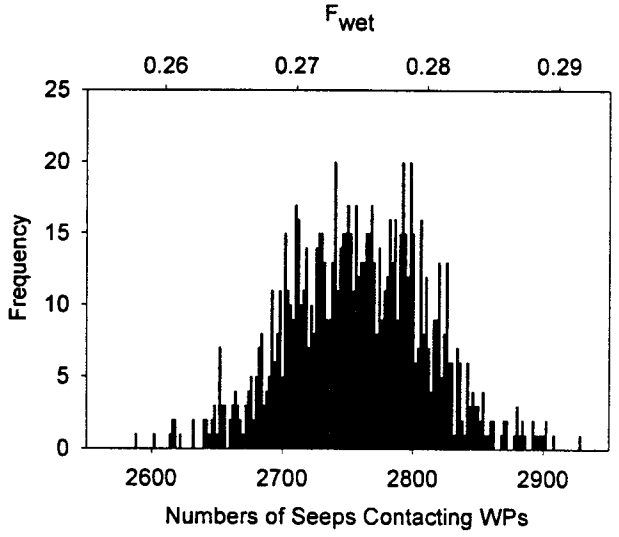

Figure 3-14. Monte Carlo simulations of the numbers of seeps contacting waste packages (WPs) and fraction of wetted WPs, F_{wet}, based on intervals between features in the Exploratory Studies Facility identified as faults, fracture zones, and shear zones

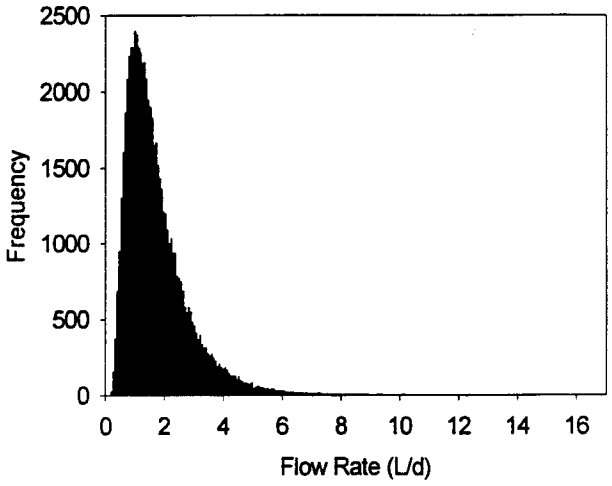

Figure 3-15. Histogram of flow rates from a single Monte Carlo realization using frequency of preferential flow based geologic features in the Exploratory Studies Facility identified as faults, fracture zones, and shear zones

4 FLUX IN THE FRACTURE NETWORK INFERRED FROM SECONDARY MINERALS

4.1 CALCITE-OPAL DEPOSITS IN THE EXPLORATORY STUDIES FACILITY

Staff from the USGS working on the YMP proposed using secondary mineralization (calcite and opal deposits) in lithophysal cavities and fracture openings as a natural analog for seepage into waste emplacement drifts (Marshall et al., 1999). This idea is attractive because calcite and opal deposits provide a record of mineral deposition from unsaturated flow through the repository horizon on a time scale of millions of years. Predominantly calcite with admixed opal deposits occurs as thin coatings in fractures and as deposits on the floors of lithophysal cavities (Paces et al., 1996). Secondary minerals in fractures generally occur only where apertures exceed several millimeters. This occurrence is probably because sufficient airflow is required for evaporation to cause supersaturation and calcite precipitation. Capillary and film flows through hairline fractures probably do not precipitate calcite because of restricted airflow and evaporation. Thicker coatings are more common on low-angle fractures. Calcite is present in both high- and low-angle fractures. Secondary minerals, however, are invariably absent on the hangingwalls of high-angle fractures (Paces et al., 1996). Deposits in lithophysal cavities are commonly 2–3 cm thick and occur only on the floors of lithophysal cavities, never on the walls or ceilings (Paces et al., 1996). Lithophysal cavities hosting secondary minerals are almost always intersected by thin-aperture fractures. Sites having elevated, bomb pulse, $^{36}Cl/Cl$ ratios typically lack extensive secondary mineralization. This observation and the absence of young aged minerals associated with these sites suggest that flux responsible for bomb pulse ^{36}Cl is not related to the fluids responsible for mineral deposition.

Paces et al. (1996) investigated age distributions of secondary mineral occurrences by radiocarbon and uranium-series disequilibrium dating techniques. Samples for $^{230}Th/U$ dating were collected from the outermost surfaces of opal and calcite, generally limited to a few tenths of a millimeter in thickness. Nearly all of these dates were less than 400 ka, much less than the 12.7 Ma postdepositional history of the formation. These data also indicate that lithophysal cavities experience approximately the same fluxes as fractures (Paces et al., 1996). Assumptions used in radioisotope dating of the secondary minerals involve a model of either episodic, instantaneous deposition or slow, continuous deposition. Age discrepancies between the younger radiocarbon dates and older $^{230}Th/U$ dates cannot be explained by the episodic deposition model but are predicted by the continuous deposition model (Paces et al., 1996). Also $^{230}Th/U$ ages are fairly uniformly distributed throughout the last 400 ka rather than clustered around discrete episodes of mineral deposition. Geochronology using radiocarbon and uranium-series dating methods suggests a slow and relatively constant rate of mineral deposition on the order of 1–5 mm per million years (Paces et al., 1997, 1998a,b). Presuming that secondary mineral deposition is linked to percolation flux, these data are consistent with a conceptual model of flux through the fracture network buffered from variations in net infiltration except in zones of vertically connected high permeability.

4.2 SEEPAGE FLUX ESTIMATES BASED ON CALCITE-OPAL DEPOSITS

Marshall et al. (1999)[1] estimate upper (7.3 mm/yr) and lower (0.003 mm/yr) bounds on the percolation flux based on secondary mineral abundances extrapolated from line measurements in the ESF between stations 11 + 00 and 30 + 00. Model parameters of Marshall et al. (1999)[2] evolved from early implementations (Paces et al., 1996, 1997) as the approach was refined. However, all reported estimates rely on the underlying assumption that the secondary calcite and opal observed in fractures and lithophysal cavities formed at a constant rate since the establishment of a fracture system capable of sustaining flow (~10 Ma), which is consistent with isotopic evidence discussed previously. Two additional model assumptions, that the flux rate and the composition of the infiltrating water also remained constant throughout that same time period, constitute the simplest explanation for the first assumption. Percolation fluxes were estimated by placing constraints on the composition of the infiltrating water and the fraction of Ca^{2+} incorporated into calcite, calculating the volumetric water/rock ratio required to account for estimated calcite abundances and fixing the time required for calcite precipitation. Bounding flux values were estimated by varying the composition of the infiltrating water and the efficiency with which Ca^{2+} is incorporated into calcite.

A minimum percolation flux (0.003mm/L) was estimated by introducing assumptions that reduce the volume of infiltrating water required to account for the mass of observed calcite.[3] To accomplish this, it was assumed that all water reaching a lithophysal cavity evaporated and all the Ca^{2+} precipitated as calcite. Another way to minimize the volume of infiltrating water is to maximize the Ca^{2+} concentration of the infiltrating solution. It would not be realistic, however, to set the Ca^{2+} concentration arbitrarily high because calcite equilibrates rapidly and extreme degrees of supersaturation are difficult to explain. The latest approach of the USGS[4] is to fix the concentration of Ca^{2+} in the infiltrating solution at 60 mg/L, roughly twice the concentration required to equilibrate calcite under atmospheric [0.03 % CO_2 (g)] and slightly alkaline pH conditions. This is a justifiable upper bound on the Ca^{2+} concentration because it is consistent with the calcite saturation states calculated for some YM pore waters (Browning et al., 1999). These assumptions provide a reasonable lower bound on the percolation flux required to account for secondary mineralization in the ESF.

An upper bound on the percolation flux into the drift (7.3 mm/yr.) was calculated by introducing assumptions that increase the volume of infiltrating water required to account for the mass of observed calcite (Marshall et al., 1999). Because calcite is a common secondary mineral at YM and equilibrates rapidly, the infiltrating waters should remain close to saturation with respect to calcite, which is consistent with the calculations of Browning et al. (1999). Marshall et al. (1999) fix the concentration of calcium in the infiltrating waters at 10 mg/L, roughly half the amount required for calcite equilibria at surface conditions and significantly less than the measured Ca^{2+} concentrations from either the J-13 well or from pore waters extractions from YM (Harrar et al., 1990; Yang et al., 1996, 1998). Estimates of the percolation flux were increased further by assuming that only half the Ca^{2+} in the infiltrating waters was incorporated into calcite.

---

[1] Marshall, B.D., L.A. Neymark, J.B. Paces, Z.E. Peterman, and J.F. Whelan. Seepage flux conceptualized from secondary calcite in lithophysal cavities in the Topopah Spring Tuff, Yucca Mountain, Nevada. *Proceedings of the Society for Mining, Metallurgy, and Exploration, Inc. Annual Meeting and Exhibit, February 28-March 1, 2000.* [additional information] Littleton, CO: Society for Mining, Metallurgy, and Exploration, Inc. Accepted for publication. 2000.

[2] Ibid.

[3] Ibid.

[4] Ibid.

The approach of Marshall et al. (1999) may not result in a useful upper bound for the percolation flux, however, because the fraction of the total available Ca^{2+} assumed to have precipitated as calcite appears arbitrarily high. For the case where advection is more efficient than *in situ* evaporation, a significantly lower fraction is possible. The underlying assumption of the Marshall et al. (1999)[5] and Paces et al. (1996) models is that calcite was deposited continuously since the beginning of fracture flow. This assumption implies that the percolating solution maintained a fixed degree of supersaturation with respect to calcite for ~10 Ma. The rate that Ca^{2+} is incorporated into calcite is proportional to the saturation state of the solution with respect to calcite and, for an advection dominated system, the fraction of the total Ca^{2+} that will precipitate as calcite is also proportional to the saturation state. Isotopic and petrologic evidence for slow calcite growth, the ability of calcite to equilibrate quickly in solutions, and calculated calcite saturation states (Log Q/K) of nearly 0 for pore waters (Browning et al., 1999) all point to low degrees of supersaturation. Assuming that advection dominates evaporation, this evidence implies that the largest fraction of the total available Ca^{2+} may have percolated downward through the rock without precipitating as calcite.

Additional analysis is needed to define a reasonable upper bound on the percolation flux. One way to accomplish this, as suggested previously, is to assume an advection dominated system and low degrees of supersaturation with respect to calcite. Still more precise estimates can be made by using analytical water compositions from YM to define the infiltrating water composition (Yang et al., 1996, 1998) rather than relying on estimates (Marshall et al., 1999)[6]. In addition, measured pore water compositions from both above and below the TSw can be used to constrain the actual extent of Ca^{2+} loss in the TSw. Finally, measured changes in the concentration of pore waters with depth can be used to estimate evaporation rates and place constraints on the percolation flux for liquid flux pathways that do not coincide with evaporation pathways (preferential flow paths).

Given the large range between proposed upper and lower bounds on the percolation flux, it is also useful to consider the best estimate on the percolation flux (2 mm/yr).[7] Using the geochemical code PHREEQC (Parkhurst, 1995), Marshall et al. (1999)[8] estimate different water compositions for the PTn and TSw based on the sensible assumptions that calcite- and opal-saturated surface water becomes progressively more evaporated and encounters higher temperatures and lower partial CO_2 (g) gas pressures with depth. Measured CO_2 gas pressures from boreholes at YM and reasonable estimates of the geothermal gradient were used to constrain the model (Thorstenson et al., 1990). However, estimates of the extent of evaporation with depth are highly model dependent, and no reference or discussion is presented in the text to justify the choice of evaporation parameters used in the model. Yet, it is clear from the text that the model assumes a single extent of evaporation throughout both the PTn and the TSw. If, instead, the extent of evaporation varies significantly across geologic formations with large thicknesses, then the use of a fixed percent evaporation for each geologic formation could contribute significant uncertainties to the model results. Because both evaporation and percolation are time-dependent processes, best estimates of the percolation flux would be refined if a relationship could be drawn between the relative rates of evaporation and percolation with depth. Measured variations in the concentrations of pore waters with depth ought to provide some insight to bound

---

[5] Marshall et al. Seepage flux conceptualized ... 2000.

[6] Ibid.

[7] Ibid.

[8] Ibid.

these rates. Further refinement of the model may be accomplished by accounting for additional Ca^{2+} supplied by the equilibration of Ca-bearing glasses and feldspars in the rock (Broxton et al., 1987). Marshall et al. (1999)[9] assume that all Ca^{2+} is supplied by the percolating water, which tends to overestimate the volume of water required to account for the estimated mass of observed calcite.

4.3 FRACTION OF WASTE PACKAGES AFFECTED BY FRACTURE NETWORK SEEPAGE FLUX

Seepage flux through the distributed, interconnected fracture network may be fairly ubiquitous in the Topopah Spring welded units but still sufficiently heterogeneous that it will not affect all WPs. In this section, an estimate of the fraction of WPs potentially contacted by the flux rates described in section 4.2 is obtained by analysis of secondary mineral deposit data from the detailed line survey of the ESF. It is assumed that the frequency of secondary mineral deposits in the ESF corresponds to the frequency of seeps that may potentially affect WPs. Individual survey intervals were 0.6-m-wide, 30-m-long bands along the right rib of the ESF about 1.2–1.7 m above the concrete invert (Paces et al., 1998). Survey intervals were centered at 100-m construction stations starting from the North Portal at CS 1 + 00 and extending to CS 71 + 00. Data used in this analysis start at CS 12 + 00, because this is the first 100-m CS within the TSw. Thickness and width of individual calcite and opal deposits were summed and divided by the area of the band to obtain mineral abundances. Only the number of calcite and opal deposits within each 30-m interval is used here to estimate fraction of WP potentially affected. Note that the ESF line survey data used here is summary data. The analysis and results presented here will be modified and improved with the detailed data as soon as this full data set is received from the USGS.

Data of the number of deposits per 30-m survey interval are shown in figure 4-1 as an empirical CDF. If the secondary mineral deposits were distributed with uniform density, then the number occurring within a given interval should have a Poisson distribution (Papoulis, 1965). The data, however, appear exponential. The discrete analogue of the exponential distribution is the geometric distribution describing a series of independent trials having equal probability of success. The solid line in figure 4-1 is the distribution function of a geometric random variable with parameter $p = 0.15$. While it is difficult to explain why these data should appear to have a geometric distribution, using them to simulate secondary mineral deposits along drifts is straightforward. The total length of the emplacement drift was divided into 30-m segments, and a realization was drawn from a geometric distribution with $p = 0.15$. This distribution was determined by generating uniform random numbers on the interval (0,1) until one was less than or equal to 0.15. The number of uniform deviates drawn before this occurred was taken to represent the number of secondary mineral deposits in that 30-m interval. Results of a single simulation of numbers of deposits per 30-m intervals over the total length of emplacement drifts are shown in figure 4-2 compared to a geometric distribution with parameter $p = 0.15$. Figure 4-2 shows that the simulation produces results with a distribution comparable to the data in figure 4-1.

The detailed line survey data (Paces et al., 1998a,b) give only the number of secondary mineral deposits occurring in specific 30-m intervals and no information on distribution of those deposits within intervals. Information on deposit location within each interval is contained in the full data set and has been

[9] Marshall et al. Seepage flux conceptualized ... 2000.

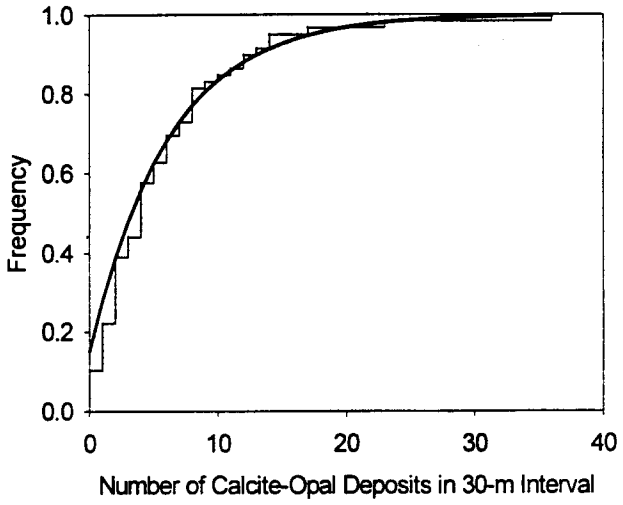

Figure 4-1. Sample cumulative distribution function of number of secondary mineral deposits in the 30-m intervals of the detailed line survey of the Exploratory Studies Facility. The solid line is a geometric distribution function with parameter p = *0.15*.

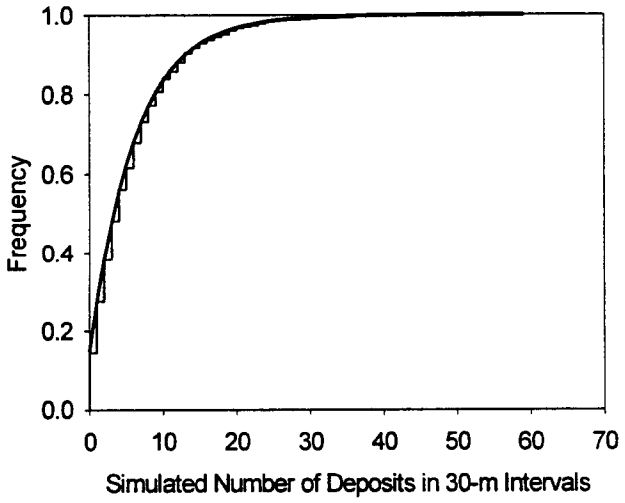

Figure 4-2. Simulated cumulative distribution function of number of secondary mineral deposits per 30-m interval compared to a geometric distribution function with parameter $p = 0.15$

requested from the USGS. To interpolate from 30-m intervals to the scale of WPs, the following conservative assumption was used. The number of WPs potentially contacted by seeps was set equal to the number of deposits simulated within a 30-m interval when the number of simulated deposits was less than or equal to 6 and set to 6 when the number of simulated deposits was greater than 6. Figure 4-3 shows the results of 10,000 realizations of simulations, where the simulation shown in figure 4-2 is one realization. The average number of affected WPs from these simulations is 5,886 with standard deviation 95. For 10,039 WPs in the repository, this average and standard deviation produce a fraction of affected Wps, $F_{wet} = 0.586$, with a standard deviation 0.01. This estimate is probably biased toward conservatism because of the assumptions that every observed secondary mineral deposit corresponds to a potential seep and that these seeps are evenly spaced within the 30-m intervals.

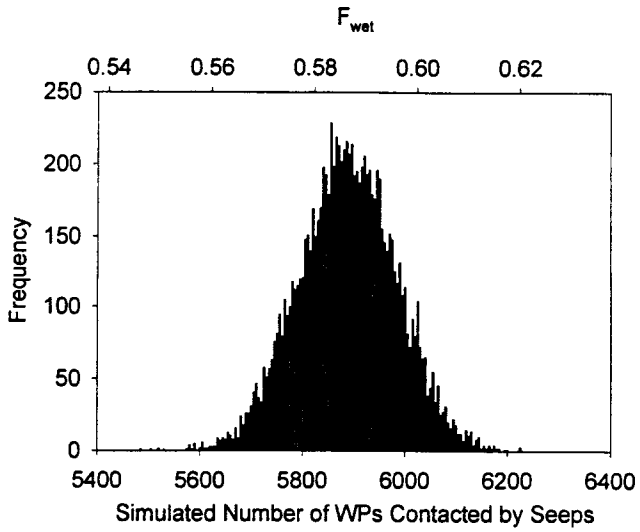

Figure 4-3. Simulated number of waste packages (WPs) potentially contacted by seeps assumed to correspond to occurrences of calcite-opal deposits

5 DISCUSSION AND RECOMMENDATIONS

5.1 DISCUSSION

Forming the foundation of this report and its recommendations is a conceptual model of deep percolation through the unsaturated TSw occurring in three distinct modes. These three modes are flow through the matrix of the welded tuff, flow through an interconnected fracture network, and flow through preferential pathways along zones of vertically connected high permeability. Flow rates in each of these modes are related according to Eq. (3-4). This conceptual model is not dependent on the actual mechanisms of flow and deliberately is parsimonious to be easily adapted to, and constrained by, additional information. Distributions of seepage catchment areas are estimated here based on the frequency of bomb pulse ^{36}Cl and structural features in the ESF. These distributions possibly may be further constrained by topography and more data on through-going geologic features. It is anticipated that new developments in constitutive models for unsaturated flow in fractures will improve estimates of potential flow through preferential pathways and also help to constrain the distribution of seepage catchment areas. Flow through the welded matrix can be estimated from saturated matrix permeabilities, and flow through the fracture network may be reasonably bounded by estimates based on secondary mineralization. Estimates of the upper bound on flow through the fracture network may be significantly improved by the suggestions in section 4.2. Based on these constraints, partitioning of flow through different modes can be balanced by Eq. (3-4). Flux through the matrix is considered to have no effect on WPs or repository performance because it is small and strongly held in the matrix by capillarity. Water is postulated here to potentially enter the emplacement drifts by two distinctly different pathways. Flow in preferential conduits intersecting drifts near the crown is postulated to potentially form locally saturated zones and drip directly onto WPs. This type of flow, as discussed in section 3.4, is likely to affect only a small fraction of WPs. Observations of secondary mineralization in lithophysal cavities suggest that seepage through the distributed fracture network may not drip. If seepage through the fracture network dripped into lithophysal cavities, it should leave calcite deposits on the cavity ceilings or walls, and none were observed (Paces et al., 1996). If water undersaturated with calcite were dripping into cavities where later evaporation caused mineral precipitation, it would be necessary to explain how that water was undersaturated. Flow through the fracture network does, however, enter subterranean cavities as demonstrated by calcite deposits on the floors of lithophysal cavities. Thus, this flux should be considered, but may have a distinctly different impact on repository performance than water that drips directly onto WPs. Recent data have led the USGS to reconsider whether or not water may drip into lithophysal cavities. Some evidence of drip store has recently been found, and the USGS now thinks dripping into some lithophysal cavities may have occurred.[1]

5.2 RECOMMENDATION

PA parameters for the fraction of affected WPs, F_{wet}, and flow rate, F_{ow}, should be implemented so that water with potential to drip and water entering drifts by mechanisms other than dripping are included.

The analyses presented in this report should be considered preliminary. With this in mind, recommendations for PA parameters of potentially dripping water are made as follows. The fraction of

---

[1] Marshall, B.D., L.A. Neymark, J.B. Paces, Z.E. Peterman, and J.F. Whelan. Seepage flux conceptualized from secondary calcite in lithophysal cavities in the Topopah Spring Tuff, Yucca Mountain, Nevada. *Proceedings of the Society for Mining, Metallurgy, and Exploration, Inc. Annual Meeting and Exhibit, February 28–March 1, 2000.* Littleton, CO: Society for Mining, Metallurgy, and Exploration, Inc. Accepted for publication. 2000.

affected WPs may be reasonably well described by a normal distribution with a mean of approximately 0.01 for present day climate up to 0.27 for wet climate conditions. The mean fraction of affected WPs for preferential flow with dripping potential is strongly correlated to net infiltration. However the standard deviation of fraction of affected WP is not, ranging only from about 0.001 up to 0.005. Flow rates onto WPs from preferential flow paths remain highly uncertain. This uncertainty is a top priority for improving the model. Preferential flow rates for present day climate conditions are estimated to be lognormal with a mean of the natural log of flow in L/d of about -0.23. Flow rates in preferential pathways are correlated with net infiltration, but not strongly because increased infiltration may follow new pathways rather than increasing flow in an existing pathway. Data from Alcove 1 show the number of flow paths increase with increasing infiltration up to a point after which flow rate in existing flow paths increases while the number remains fairly constant.(Fedors, 1998).[2] For wetter climate conditions, a preliminary estimate for the mean of the natural log of flow in L/d is 0.35. Standard deviation of flow rates in preferential pathways appears to be uncorrelated with net infiltration, remaining at around 0.6 for the natural log of flow in L/d.

Based on evidence of secondary mineralization, flux in the distributed fracture network is conceptualized to be correlated only weakly with net infiltration. Actual flow rates, however, remain highly uncertain with estimates from the USGS ranging over 4 orders of magnitude, from a minimum of 0.003 mm/yr to a plausible maximum of 7.3 mm/yr. Further analyses of existing data, as suggested in section 4.2, may reduce this uncertainty, providing reasonable best and upper bound estimates. For present day climate conditions, using the upper bound of flux through the fracture network would result in almost no flow in preferential pathways and, using the lower bound, almost all flow would follow preferential pathways. Implementing both modes of flow, coupled through Eq. (3-4), is postulated here to be a reasonably realistic conceptual model of unsaturated flow at YM. While the flow rates through the fracture network remain highly uncertain if secondary mineral deposits represent the occurrence of seeps in the fracture network, then the fraction of WPs potentially affected by fracture network flux appears fairly well constrained. Simulations based on observations of secondary mineral deposits in the ESF indicate that the fraction of WPs affected by this mode of flow can be characterized as normally distributed with a mean 0.586 and standard deviation 0.01. Perhaps this fraction is somewhat correlated with net infiltration, but is not seen because mineral deposits reflect the long-term average net infiltration.

As is the case with most models, this approach is a major simplification of reality and suffers with problems of model validation and unverifiable assumptions. On the other hand, its advantages are its simplicity, parsimonious parameterization, relative ease of modification, and facility for incorporating various types of data. The essential idea is to relate only the mean and variance of data, such as occurrence of bomb pulse ^{36}Cl or secondary mineral deposits, to the mean and variance of some event, in this case, dripping onto WPs. Transfer of statistical moments was based on tesselation for the preferential flow paths and the assumption that the occurrences of secondary mineral deposits are equivalent to prevalence of seeps for fracture network flow. It should be understood that the general methodology does not depend on these particular transfer assumptions. Further it should be obvious that, although the methodology is cast in probabilistic terms, all uncertainties are not accounted for and, in fact, uncertainties are introduced by the transfer assumptions. Alternate transfer assumptions, perhaps based on topography and a more thorough assessment of geological controls, would perhaps help to evaluate uncertainties and improve estimates. While it may be possible to compare this approach to mechanistic process-type models, that comparison would likely not be entirely satisfactory because models could be constructed that compared either quite well or quite

---

[2] Flint, A.L. *Proceedings of the Society for Mining, Metallurgy, and Exploration, Inc. Annual Meeting and Exhibit, February 28-March 1, 2000.* Littleton, CO: Society for Mining, Metallurgy, and Exploration, Inc. Accepted for publication. 2000.

poorly depending on the particular model construction. A more satisfying validation exercise would be a large-scale field infiltration test where this approach along with other process-type models, were compared against data. Such a field test would require detailed characterization of geologic features, secondary mineralization, process model parameters, and the surface application of a suite of tracers to be monitored in an underground facility. The model as presented deals only with isothermal flow. However, including penetration of the boiling isotherm mechanism through the length scale expression of Phillip (1996) is a straightforward modification of the proposed model for the thermal period. Effects of other coupled processes on this approach would need to be evaluated through mechanistic models of these coupled processes.

24/27

6 FUTURE WORK PRIORITIES

Estimates of the fraction of WPs affected by water seeping into emplacement drifts provided in this report are based on data collected in the ESF and conventional statistical techniques. These estimates can be refined easily as more data become available from the ECRB and ESF. Estimates of flow rates onto WPs, on the other hand, are highly uncertain and speculative. Work is currently in progress to revise the Yang et al. (1999) constitutive models for unsaturated flow through fractures as an additional constraint on flow through preferential pathways and associated seepage catchment areas. The USGS model (Marshall et al., 1999)[1] of flux through the distributed fracture network uses assumptions that may result in an unrealistically low lower bounding estimate and also may underestimate the upper bound. As stated in section 4.2, some of these assumptions can be replaced with actual data, and the model may otherwise be improved to obtain more reliable bounding and best estimates. Efforts to decrease uncertainty in the estimates of deep percolation flux should be considered top priority for improving this model.

Data expected to be collected from the ECRB should provide critical information regarding the presence and frequency of preferential flow pathways. It also may be possible to determine from drip-cloth in the ECRB whether or not flux through the distributed fracture network will drip into drift-sized openings. It is difficult to translate petrographic information from secondary mineral deposits in lithophysal cavities to emplacement drifts because scale effects. If dripping from vapor condensation can be distinguished from dripping from fractures, then data collected in the ECRB may help to address the question of dripping from the distributed network of fractures. Reliable estimation of seepage into drifts depends on understanding the mechanisms of unsaturated flow through the TSw and linking data from surface infiltration maps to deep percolation.

[1] Marshall, B.D., L.A. Neymark, J.B. Paces, Z.E. Peterman, and J.F. Whelan. Seepage flux conceptualized from secondary calcite in lithophysal cavities in the Topopah Spring Tuff, Yucca Mountain, Nevada. *Proceedings of the Society for Mining, Metallurgy, and Exploration, Inc. Annual Meeting and Exhibit, February 28–March 1, 2000.* Littleton, CO: Society for Mining, Metallurgy, and Exploration, Inc. Accepted for publication. 2000.

7 REFERENCES

Birkholzer, J., G. Li, C.-F. Tsang, and Y.Tsang. Modeling studies and analysis of seepage into drifts at Yucca Mountain. *Journal of Contaminant Hydrology* 38(1–3): 349–384. 1999.

Bodvarsson, G.S., T.M. Bandurraga, and Y.S. Wu. *The Site-Scale Unsaturated Zone Model of Yucca Mountain, Nevada, for the Viability Assessment.* LBNL–40376, UC–814. Berkeley, CA: Lawrence Berkeley National Laboratory. 1997.

Boles, J.R. Calcite precipitates in the Mission Tunnel: A 90-year record of groundwater seeps in fractured sandstone. *EOS, Transactions, American Geophysical Union* 80(46): F423. 1999.

Browning, L., W.M. Murphy, B.W. Leslie, and W.L. Dam. Thermodynamic interpretations of chemical analyses of unsaturated zone water from Yucca Mountain, Nevada. *Materials Research Society Symposium Proceedings, 1999 Fall Meeting.* Warrendale, PA: Materials Research Society. 1999.

Broxton, D.E., D.L. Bish, and R.G. Warren. Distribution and chemistry of diagenetic minerals at Yucca Mountain, Nye County, Nevada. *Clays and Clay Mineralogy* 35(2): 89–110. 1987.

Chandler, N., C.C. Davison, G. Gee, P. LaPointe, and S. Neuman. Drift Seepage Peer Review Panel Report: *Consensus Peer Review of Drift Seepage at Yucca Mountain.* Preliminary Draft Copy. Yucca Mountain Project. Las Vegas, NV: Yucca Mountain Project Office 1999.

Chen, G., M. Taniguchi, and S.P. Neuman. *An Overview of Instability and Fingering During Immiscible Fluid Flow in Porous and Fractured Media.* NUREG/CR–6308. Washington, DC: Nuclear Regulatory Commission. 1995.

Chen, R. Analysis of drift stability and rockfall due to earthquake ground motion at Yucca Mountain, Nevada. *Proceedings of the 37th U.S. Rock Mechanics Symposium, June 6–9, 1999.* Vail, CO: American Rock Mechanics Association: 759–766. 1999.

Chesnut, D.A. Characterizing the altered zone at Yucca Mountain: The beginnings of a testing strategy. *Proceedings of the Third International Conference on High-Level Radioactive Waste Management.* La Grange Park, IL: American Nuclear Society: 1,663–1,670. 1992.

Civilian Radioactive Waste Management System, Management & Operating Contractor. *Total System Performance Assessment—Viability Assessment (TSPA-VA) Analyses Technical Basis Document.* B00000000–01717–4301–00007. Revision 00. Las Vegas, NV: TRW Environmental Safety Systems Inc. 1998a.

Civilian Radioactive Waste Management System, Management & Operating Contractor. *Peer Review Report on Chlorine-36 Studies at Yucca Mountain.* Las Vegas, NV: Office of Civilian Radioactive Waste Management System, Management & Operating Contractor. 1998b.

Deutsch, C.V., and A.G. Journel. *GSLIB: Geostatistical Software Library and User's Guide.* Oxford, NY: Oxford University Press. 1992.

Dexter, A.R. Heterogeneity of unsaturated gravitational flow of water through beds of large particles. *Water Resources Research* 29(6): 1,859–1,862. 1993.

Eaton, R.R., C.K. Ho, R.J. Glass, M.J. Nicholl, and B.W. Arnold. *Three-Dimensional Modeling of Flow Through Fractured Tuff at Fran Ridge.* SAND95–1896, UC–814. Albuquerque, NM: Sandia National Laboratories. 1996.

Fabryka-Martin, J.T., A.L. Flint, D.S. Sweetkind, A.V. Wolfsberg, S.S. Levy, J.L. Roach, G. Woldegabriel, and L.E. Wolfsberg. *Evaluation of Flow and Transport Models of Yucca Mountain Based on Chlorine-36 Studies for FY97.* LA–CST–TIP–97–010, LANL Milestone SP2224M3. Los Alamos, NM: Los Alamos National Laboratory. 1997.

Fairhurst, C. Rock mechanics and nuclear waste repositories. *Proceedings of the 37th U.S. Rock Mechanics Symposium, June 6–9, 1999.* Vail, CO: American Rock Mechanics Association: 1–43. 1999.

Fedors, R.W. *Trip Report for Second Annual Workshop on Field Testing and Associated Modeling of Potential High-Level Nuclear Waste Geologic Disposal Sites.* San Antonio, TX: Center for Nuclear Waste Regulatory Analyses. 1998.

Finsterle, S. *ITOUGH2 User's Guide.* LBNL–40040. Berkeley, Ca: Lawrence Berkeley National Laboratory. 1999.

Finsterle, S., and R.C. Trautz. *Seepage Calibration Model and Seepage Testing Data: Analysis/Model Report U0080 MDL–NBS–HS–000004.* Revision 00D. Las Vegas, NV: Office of Civilian Radioactive Waste Management System, Management & Operating Contractor. 1999.

Gauthier, J.H. An updated fracture-flow model for Total-System Performance Assessment of Yucca Mountain. *Proceedings of the Fifth Annual International Conference on High-Level Radioactive Waste Management.*: La Grange Park, IL: American Nuclear Society: 1,663–1,670. 1994.

Harrar, J.E., J.F. Carley, W.F. Isherwood, and E. Raber. *Report of the Committee to Review the Use of J-13 Well Water in Nevada Nuclear Waste Storage Investigations.* UCID–21867. Livermore, CA: Lawrence Livermore National Laboratory. 1990.

Haukwa, C.B. *AMESH: A Mesh Creating Program for the Integral Finite Difference Method.* Berkeley, CA: Earth Sciences Division. Lawrence Berkeley National Laboratory. 1998.

Hughson, D.L. *Trip Report to Las Vegas—Drift Seepage Peer Review.* San Antonio, TX: Center for Nuclear Waste Regulatory Analyses. 1999.

Hughson, D.L., T. Maxwell, and R. Green. Dripping threshold from a glass plate hele-shaw fracture analog. *EOS, Transactions, American Geophysical Union* 80(46): F468. 1999.

Jury, W.A. Simulation of solute transport using a transfer function model. *Water Resources Research* 18(2): 363–368. 1982.

Jury, W.A., and K. Roth. *Transfer Functions and Solute Movement through Soil: Theory and Applications,* Basel, Switzerland: Birkhäuser Verlag. 1990.

Klute, A., ed. *Methods of Soil Analysis. Part 1: Physical and Mineralogical Methods.* 2nd Edition. Madison, WI: American Society of Agronomy Inc. and Soil Science Society of America Inc. 1986.

Marshall, B.D., L.A. Neymark, J.B. Paces, Z.E. Peterman, and J.F. Whelan. Seepage flux conceptualized from secondary calcite in lithophysal cavities in the Topopah Spring Tuff, Yucca Mountain, Nevada. *EOS, Transactions, American Geophysical Union* 80(17): S5. 1999.

Murphy, W.M. Commentary on Studies of ^{36}Cl in the Exploratory Studies Facility at Yucca Mountain, Nevada. *Materials Research Society Symposium Proceedings.* Warrendale, PA: Materials Research Society 506: 407–414. 1998.

Nicholl, M.J., and R.J. Glass. Effective media models for unsaturated fractured rock: A field experiment. *Proceedings of the Sixth Annual International Conference on High-Level Radioactive Waste Management.* La Grange Park, IL: American Nuclear Society: 39–40. 1995.

Nuclear Regulatory Commission. *Issue Resolution Status Report (Key Technical Issue: Unsaturated and Saturated Flow Under Isothermal Conditions).* Revision 1. Washington, DC: U.S. Nuclear Regulatory Commission. 1998.

Paces, J.B., L.A. Neymark, B.D. Marshall, J.F. Whelan, and Z.E. Peterman. *Ages and Origins of Subsurface Secondary Minerals in the Exploratory Studies Facility (ESF).* Yucca Mountain Project Milestone Report 3GQH450M. Las Vegas, NV: Yucca Mountain Project Office. 1996.

Paces, J.B., B.D. Marshall, J.F. Whelan, and L.A. Neymark. *Geochronology of Fracture Fill Material, ESF & Estimated Past Water Fluxes.* Yucca Mountain Project Level 4 Milestone SPC23FM4. Las Vegas, NV: Yucca Mountain Project Office. 1997.

Paces, J.B., L.A. Neymark, B.D. Marshall, J.F. Whelan, and Z.E. Peterman. Inferences for Yucca Mountain unsaturated-zone hydrology from secondary minerals. Proceedings of the Eighth International Conference on High-Level Radioactive Waste Management Las Vegas, Nevada, May 11–14, 1998. La Grange Park, IL: American Nuclear Society: 36–39. 1998a.

Paces, J.B., B.D. Marshall, J.F. Whelan, L.A. Neymark, and Z.E. Peterman. *Summary of Calcite and Opal Deposits in the Exploratory Studies Facility and Estimates of the Distribution and Isotopic Compositions of These Minerals along the East-West Cross Drift Alignment, Yucca Mountain, Nevada.* Yucca Mountain Project Level 4 Milestone SPC237M4. Las Vegas, NV: Yucca Mountain Project Office. 1998b.

Papoulis, A. *Probability, Random Variables, and Stochastic Processes.* New York: McGraw-Hill Book Company. 1965.

Parkhurst, D.L. *User's Guide to Phreeqc—A Computer Program for Speciation, Reaction-Path, Advective Transport, and Inverse Geochemical Calculations.* U.S. Geological Survey Water Resources Investigations Report 95-4227. 1995.

Philip, J.R., J.H. Knight, and R.T. Waechter. Unsaturated seepage and subterranean holes: Conspectus and exclusion problem for circular cylindrical cavities. *Water Resources Research* 25(1): 16–28. 1989.

Phillips, O.M. Infiltration of a liquid finger down a fracture into superheated rock. *Water Resources Research* 32(6): 1,665–1,670. 1996.

Press, W.H., S.A. Teukolsky, W.T. Vettering, and B.P. Flannery. *Numerical Recipes in FORTRAN: The Art of Scientific Computing.* 2nd Edition. New York: Cambridge University Press. 1992.

Pruess, K. A mechanistic model for water seepage through thick unsaturated zones in fractured rocks of low matrix permeability. *Water Resources Research* 35(4): 1,039–1,051. 1999.

Pruess, K., B. Faybishenko, and G.S. Bodvarsson. Alternative concepts and approaches for modeling flow and transport in thick unsaturated zones of fractured rocks. *Journal of Contaminant Hydrology* 38: 281–322. 1999.

Ripley, B.D. *Spatial Statistics*. New York: John Wiley & Sons. 1981.

Russell, C.E. *Hydrogeologic investigations of flow in fractured tuffs, Rainier Mesa, Nevada Test Site.* Master's thesis, University of Nevada, Las Vegas, NV. 1987.

Shimojima, E., T. Tanaka, R. Yoshioka, and Y. Hoso. Seepage into a mountain tunnel and rain infiltration. *Journal of Hydrology* 147: 121–151. 1993.

Thordarson, W. *Perched Groundwater in Zeolitized-Bedded Tuff, Rainier Mesa and Vicinity, Nevada Test Site, Nevada.* U.S. Geological Survey Report TEI–862. 1965.

Thorstenson, D.C., E.P. Weeks, H.H. Haas, and J.C. Woodward. Physical and chemical characteristics of topographically affected airflow in an open borehole at Yucca Mountain, Nevada. *Proceedings of the Topical Meeting on FOCUS '89, Nuclear Waste Isolation in the Unsaturated Zone, Las Vegas, Nevada, September 17–21, 1989.* La Grange Park, IL: American Nuclear Society: 256–270. 1990.

Tokunaga, T.K., and J. Wan. Water film flow along fracture surfaces of porous rock. *Water Resources Research* 33(6): 1,287–1,295. 1997.

Tsang, C-F., and I. Neretnieks. Flow channeling in heterogeneous fractured rocks. *Reviews of Geophysics* 36(2): 275–298. 1998.

Wang, J.S.Y., P.J. Cook, R.C. Trautz, R. Salve, A.L. James, S. Finsterle, T.K. Tokunaga, R. Solbau, J. Clyde, A.L. Flint, and L.E. Flint. *Field Testing and Observation of Flow Paths in Niches: Phase 1 Status Report of the Drift Seepage Test and Niche Moisture Study.* Yucca Mountain Project Level 4 Milestone Report SPC314M4. Las Vegas, NV: Yucca Mountain Project Office. 1997.

Wang, J.S.Y., P.J. Cook, R.C. Trautz, Q. Hu, and R. Salve. *In-Situ Field Testing of Processes. Analysis/Model Report U0015 ANL–NBS–HS–000005.* Revision 00E. Las Vegas, NV: Office of Civilian Radioactive Waste Management System, Management & Operating Contractor. 1999a.

Wang, J.S.Y., R.C. Trautz, P.J. Cook, S. Finsterle, A.L. James, and J. Birkholzer. Field tests and model analyses of seepage into drift. *Journal of Contaminant Hydrology* 38(1-3): 323–347. 1999b.

Yang, I.C., G.W. Rattray, and P. Yu. *Interpretation of Chemical and Isotopic Data from Boreholes in the Unsaturated Zone at Yucca Mountain, Nevada.* U.S. Geological Survey Water Resources Investigations Report 96-4058. 1996.

Yang, I.C., P. Yu, G.W. Rattray, J.S. Ferarese, and R.N. Ryan. *Hydrochemical Investigations Characterizing the Unsaturated Zone at Yucca Mountain, Nevada.* U.S. Geological Survey Water Resources Investigations Report 98-4132. 1998.

Yang, Y., D. Cesano, and A.C. Bagtzoglou. *Simulated Dripping in a Rough, Multi-Segmented Fracture Set Progress Report: Model Development and Sensitivity Analysis.* New York: Department of Civil Engineering & Engineering Mechanics, Columbia University. 1999.